Summer 2018

Iron Polypyridyl Catalysts Assembled on Metal Oxide Semiconductors for Heterogeneous Photocatalytic Hydrogen Generation

Nicholas Race
College of William and Mary - Arts & Sciences, nickrace27@outlook.com

Iron Polypyridyl Catalysts Assembled on Metal Oxide Semiconductors For Heterogeneous Photocatalytic Hydrogen Generation

Nicholas Andrew Race

Warwick, New York

Bachelor of Science, Towson University, 2015

A Thesis presented to the Graduate Faculty
of The College of William & Mary in Candidacy for the Degree of
Master of Science

Department of Chemistry

College of William & Mary
May, 2018

APPROVAL PAGE

This Thesis is submitted in partial fulfillment of
the requirements for the degree of

Master of Science

Nicholas Andrew Race

Approved by the Committee April, 2018

Committee Chair
Associate Professor William R. McNamara, Chemistry
The College of William & Mary

Professor Deborah C. Bebout, Chemistry
The College of William & Mary

Professor Robert D. Pike, Chemistry
The College of William & Mary

ABSTRACT

Artificial Photosynthesis (AP) provides a promising method for the conversion of solar energy to chemical fuel in the form of H_2 and O_2. Development of heterogeneous systems in which H_2 evolution catalysts are immobilized on metal oxide semiconductors is imperative for the large-scale implementation of AP systems. This research focuses on the immobilization of an active H_2 evolution catalyst on large band gap semiconductors for the development and optimization of a highly active photocatalytic H_2 generation system.

TABLE OF CONTENTS

ACKNOWLEDGEMENTS

I would first like to thank Dr. McNamara for his guidance and mentorship throughout my time at William & Mary. Dr. McNamara has played an integral role in my development as a researcher and in the growth of my knowledge of chemistry. It has truly been a pleasure to conduct research under his supervision. I would also like to thank all of the members of Dr. McNamara's research group that I have had the pleasure of working with over the past two years. These students are amazing young scientists and superior people that have made my time here incredibly productive and enjoyable. In particular, I would like to thank Megan Screen and Brett Barden for all of their help with our photochemistry experiments that were part of this project.

I would also like to thank Dr. Bebout and Dr. Pike for serving on my thesis committee. As Director of Graduate Studies at the time of my application to the graduate program at William & Mary, Dr. Bebout provided me with much of the information that assisted me in making the decision to join this program. In my time at the College, Dr. Pike has been an invaluable resource on all issues pertaining to life as a graduate student in his role as Director of Graduate Studies. Both Dr. Bebout and Dr. Pike have greatly enhanced my time at William & Mary through their constant kindness and compassion.

Finally, I would like to thank my family for their continued support as I have pursued my academic ambitions. All of the credit for my achievements in life is owed to them.

LIST OF TABLES

LIST OF FIGURES

Chapter 1. Introduction

Global Energy Demand

Increasing global population and per-capita energy consumption have caused the global consumption of energy to increase significantly since the Industrial Revolution.[1] This trend is highly unlikely to plateau or even slow in the coming decades. As a result of the projected population and economic growth over the next 25 years, total world energy consumption is projected to rise by 28% between 2015 and 2040, from 575 quadrillion Btu to 736 quadrillion Btu (Figure 1.1).[2] Much of this projected growth in consumption can be attributed to developing nations that are not part of the Organization for Economic Cooperation and Development (OECD), including China and India. This is because of the strong relationship between economic growth and energy consumption. In developing and emerging nations, such as those outside of the OECD, economic growth tends to be much more rapid than in developed nations.[2] In order to meet the demands of rising global energy consumption, the consumption of all fuel types outside of coal are projected to increase over the next 25 years. Although these projections forecast the fastest rate of growth for renewable sources, followed by nuclear power, fossil fuels are still expected to account for 77% of global energy consumption in 2040.[2] The continued global dependence on fossil fuels to meet growing global energy demands is problematic for many reasons.

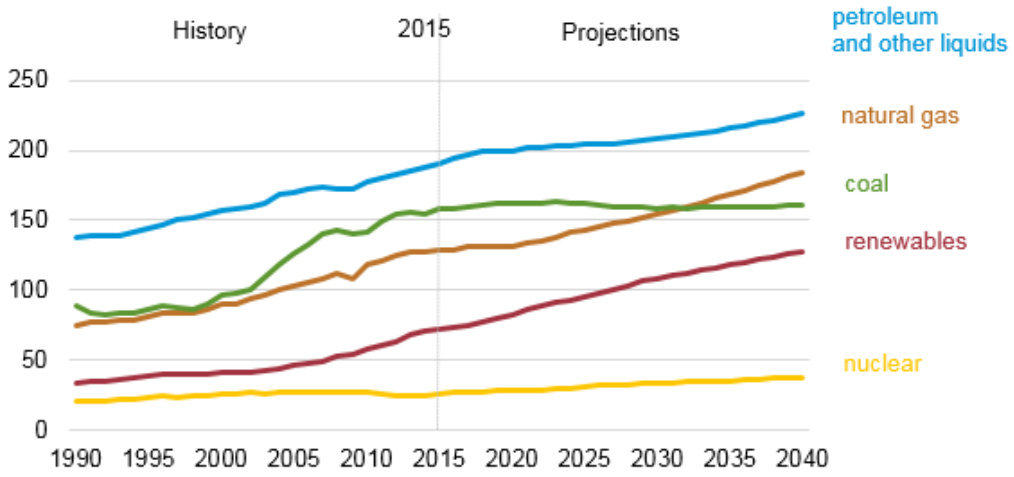

Figure 1.1. Historical and projected world energy consumption (in quadrillion Btu) by source.[2]

One of the primary issues with the continued reliance on fossil fuels as the predominant global energy source is the non-renewable nature of these fuels. In determining how far into the future global fossil fuel supplies can be sustained, it is important to make a distinction between resources and reserves. Resources, which make up the majority of global fossil fuels, are impossible or expensive to extract given current technology, or may not be fully characterized. Reserves are those supplies that are anticipated to be produced for a reasonable cost using current technology.[3] This distinction is significant because the future availability of fossil fuel reserves is highly uncertain, despite the relatively large volume of known reserves. As of 2013, the International Energy Agency projected that conventional oil reserves were sufficient to meet demand for the next 40 to 45 years at the current rate of consumption.[3] The more recently completed BP Energy Outlook was in fairly strong agreement with these projections, stating that as of 2016 global proved oil reserves were sufficient for approximately 50 years

of production at current global levels.[4] Current natural gas reserves are also projected to meet demand for approximately 50 years at the current global rate of production.[4,5] Although these projections are fairly consistent across multiple organizations, the period in which oil reserves meet demand will likely be extended by improving technology converting more resources to reserves over the next few decades. Even with improving technology allowing for the conversion of resources to reserves, it is imperative that renewable energy sources continue to account for a greater share of the global energy consumed.

Environmental Costs of Fossil Fuels and the Need for Renewable Energy

The widespread use of fossil fuels is also problematic due to the deleterious impacts that burning these fuels have on the environment. The combustion of fossil fuels releases carbon dioxide and other pollutants, such as sulfur dioxide and nitrogen oxides, into the atmosphere. Carbon dioxide emissions are particularly concerning from the outlook of climate change as a strong link has been established between CO_2 emissions and global warming.[6] Carbon dioxide is a greenhouse gas and, along with water vapor, is one of the two most abundant greenhouse gases in Earth's atmosphere.[7] These gases, along with other gases and clouds, absorb thermal radiation emitted by the Earth and reradiate back to the Earth's surface, raising the Earth's temperature. From the early industrial era through 2005, the amount of carbon dioxide in the atmosphere had increased by approximately 35%.[7] Since then, atmospheric CO_2 has continued to increase significantly, from 379 ppm in 2005 to 402.9 ± 0.1 ppm

in 2016.[7,8] In addition, the largest annual increase in global atmospheric CO_2 recorded in the 58 years of measurement occurred between 2015 and 2016.[8] The elevated levels of atmospheric CO_2 in the past few decades are particularly alarming as atmospheric CO_2 did not deviate from the range of 280 ± 20 ppm over the 10,000 years preceding the industrial revolution.[7] In addition to the rise in atmospheric CO_2, direct atmospheric measurements that have been taken since 1970 have also shown an increase in the abundance of methane and N_2O, two other known greenhouse gases.[7]

Corresponding to the rise in global atmospheric CO_2 and other greenhouse gases has been a rise in global surface temperature, illustrated by Figure 1.2. Furthering this trend, 2016 was the third consecutive year in which the record for warmest global surface temperature was set, with global land and sea temperature reaching more than 1 °C higher than average preindustrial temperatures.[8] In addition, 15 of the 16 warmest years on record occurred from 2000-2016, as measured by global surface temperature.[8]

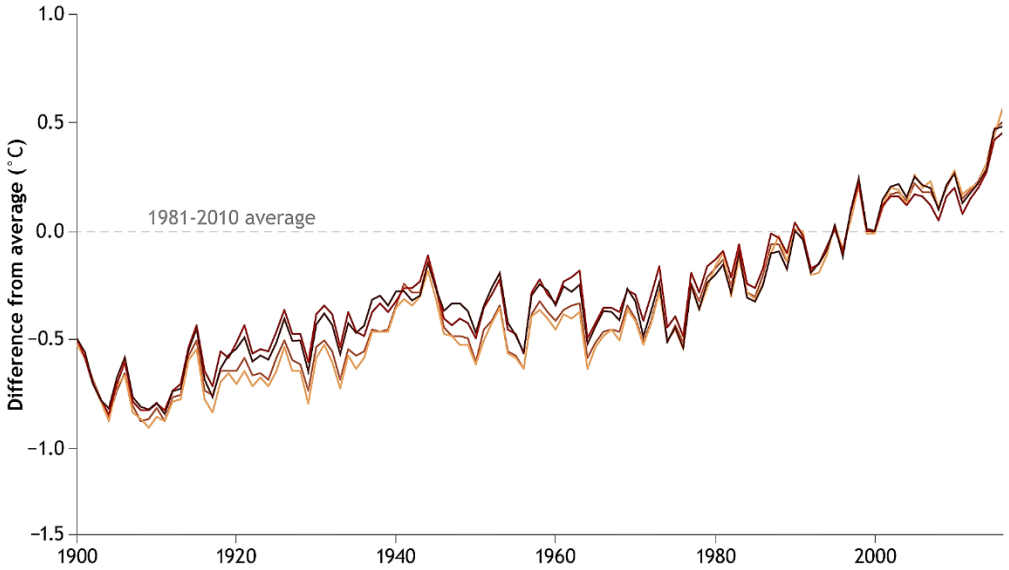

Figure 1.2. Annual global surface temperature as compared to the annual average from 1981-2010.[9]

To combat the impending shortage of fossil fuels and the detrimental impacts the burning of these fuels are having on the environment, renewable energy sources must be relied on to a greater degree. As of 2016 renewable sources accounted for 7.5% of global power generation.[4] Although this share of global power generation has grown rapidly in recent years, significant progress must still be made. The most promising source of renewable energy is solar energy. The sun provides 100,000 TW of solar energy to the Earth per year; this means that enough solar energy reaches the planet in one hour to meet human energy consumption for an entire year.[6] In order to increase the viability of solar energy as a widespread fuel source, limitations in the collection, storage, and utilization of solar energy must be overcome. Much progress has been made in utilizing solar cells to capture solar radiation and convert that energy to electricity, however these systems are not capable of storing solar energy in a form that can

be later utilized. In order for solar energy to be utilized on a much wider scale it is necessary for technologies to emerge that allow for the conversion of solar energy to fuels that can be implemented into current infrastructure.

Natural and Artificial Photosynthesis

One possible method to better utilize solar energy is to store the collected energy in chemical bonds. One example of this is the process of photosynthesis, in which solar energy and carbon dioxide are converted into chemical energy that sustains life on Earth. Photosynthesis can be divided into two related photosystems: Photosystem I (PSI) and Photosystem II (PSII) (Figure 1.3). During photosynthesis, the excited state of PSI is generated by sunlight, initiating an electron transfer process. The transferred electrons eventually reduce $NADP^+$ to NADPH, thus oxidizing PSI.[10] NADPH then serves as both the proton and electron source for the transformation of carbon dioxide into carbohydrates during the Calvin Cycle. PSI is regenerated when electrons are transferred from the excited state of PSII to the oxidized PSI. The oxidation of water to oxygen is then catalyzed by the oxidized form of PSII.[10]

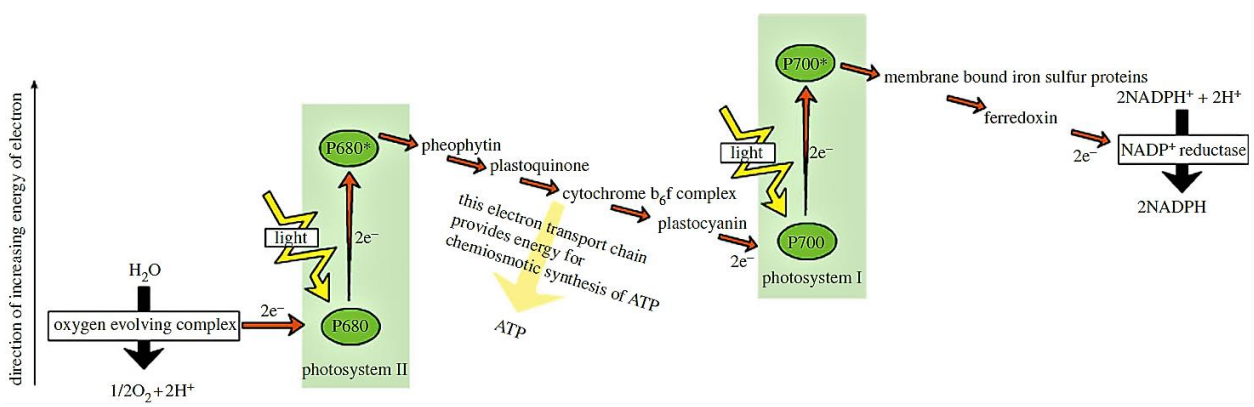

Figure 1.3. Simplified z-scheme of the light-induced reactions of photosynthesis.[6]

Inspired by natural photosynthesis, the goal of Artificial Photosynthesis (AP) systems is to convert solar energy to chemical energy through the splitting of water into molecular hydrogen and oxygen. AP systems accomplish water splitting through two redox half reactions, the reduction of aqueous protons to H_2 and the oxidation of water to O_2 (Figure 1.4). The products of these redox reactions, H_2 and O_2, are both chemical fuels that can be stored and provide energy in a renewable and environmentally-friendly manner. Rather than producing CO_2, as is the case with burning fossil fuels, the combustion of hydrogen produces only water. Because of this, AP systems may also have applications in the developing world where potable water is scarce. Hydrogen may also be fixed as a liquid fuel through hydrogenation of small molecules such as carbon dioxide, making it easier to store and transport.[11] In addition, H_2 may be used directly to power fuel cells.[11] As a result, utilizing hydrogen as a fuel source decreases the reliance on fossil fuels while also combatting the issues of increasing atmospheric CO_2 and global temperature.

$$4H^+ + 4e^- \rightarrow 2H_2 \qquad E = 0V - 0.059\ pH\ V\ vs\ NHE$$

$$\underline{2H_2O \rightarrow O_2 + 4H^+ + 4e^- \qquad E = 1.23\ V - 0.059\ pH\ vs\ NHE}$$

$$2H_2O \rightarrow 2H_2 + O_2 \qquad \Delta E = -1.23\ V$$

Figure 1.4. Redox half reactions of water splitting.

In a complete AP system the two redox half reactions would be combined, however these reactions are often studied individually to aid in the optimization of each process. The reductive half reaction of AP has typically been seen as the easier component to accomplish, as only two electrons are required compared to the four electron oxidative half reaction. However, in order for the reduction of protons to continue catalytically when separated from the oxidative half reaction, a source of electrons must be included in the system to balance the redox reaction.[12] This is typically accomplished by adding a sacrificial electron donor to the system.

Development of Homogeneous AP Systems

In order to initiate the redox half reactions of water splitting a catalyst must be incorporated into the AP system. In regards to the reductive half of an AP system, these catalysts promote the reduction of protons to H_2. Many homogeneous AP systems have been reported that incorporate a molecular proton reduction catalyst, a photosensitizer to increase visible light absorption, and a sacrificial electron donor. Unfortunately, many of these systems

incorporate catalysts or photosensitizers that contain noble metals such as platinum or ruthenium that are rare and therefore expensive. The high cost of these materials severely limits the likelihood of scaling the AP system for industrial-scale water splitting. Ideally, AP systems will incorporate catalysts that contain Earth-abundant transition metals (Fe, Co, Ni) and relatively inexpensive organic photosensitizers that allow for cost-effective implementation on a large scale.

Due to its relatively low cost and role in the active sites of some hydrogenases, nickel is of great interest for the development of AP systems. As a result, many Ni-based molecular catalysts have been reported for photocatalytic hydrogen generation. In 2012, Eisenberg and coworkers reported the synthesis of a pyridine thiolate nickel complex that mimics the [Fe-Ni]-hydrogenase active site.[13] The reported system incorporated noble-metal-free organic dyes fluorescein and Eosin Y as photosensitizers and triethylamine as the sacrificial electron donor. When combined with fluorescein and the sacrificial donor in 1:1 ethanol:water mixtures, the catalyst was found to be highly active for hydrogen generation, reaching 5500 TON after 40 hours of irradiation.[13] At the time of publishing, this system was more active than any previously reported noble-metal-free homogeneous system.[13] Holland et al. have also reported a system for photocatalytic hydrogen generation incorporating a nickel(II) phosphine complex as the proton reduction catalyst.[14] This system initially utilized Eosin Y as the photosensitizer and ascorbic acid as the sacrificial donor species in 1:1 mixtures of acetonitrile:water. However, it was found that the Eosin Y

decomposed rather quickly within the system. As a result, $[Ru(bpy)_3]Cl_2$ and ascorbic acid had to be added to the catalyst mixture during photolysis in order for the system to reach its maximum activity of 2700 TON over 150 hours.[14] Although it was reported that the catalyst did not degrade over the course of photolysis, the need to incorporate the ruthenium photosensitizer to optimize the activity of the system limits the likelihood of utilizing this system on a large scale.

There have also been numerous cobalt catalysts reported for photocatalytic hydrogen generation in homogeneous AP systems. In 2009 Eisenberg et al. reported a series of cobaloxime complexes that were found to be active for photocatalytic H_2 evolution in aqueous mixtures of acetonitrile utilizing triethanolamine as the sacrificial donor species.[15] The most active catalyst of the cobaloxime complexes was found to reach approximately 2150 TON after only 10 hours of irradiation.[15] However, this system utilized a platinum terpyridyl acetylide chromophore and the reaction mixture was a ratio of 24:1 acetonitrile:water.[15] Both of these aspects would significantly increase the cost of a larger scale AP system, limiting the utility of the catalyst. Eisenberg and coworkers have since been successful in improving this system through the incorporation of ligands functionalized with electron withdrawing groups. The most active cobalt-dithiolene complex generated up to 9000 TON when paired with the photosensitizer $Ru(bpy)_3^{2+}$ and sacrificial donor ascorbic acid.[16] In addition to demonstrating increased catalytic activity, the improved system incorporated a less expensive photosensitizer and the reaction mixture was 1:1 acetonitrile:water, addressing two of the largest deficiencies of the cobaloxime

system.[16] Bernhard and coworkers have also reported a cobalt complex, $[Co(bpy)_3]Cl_2$, that is active for photocatalytic H_2 generation from aqueous mixtures.[17] This system incorporated triethanolamine as the sacrificial donor species and a series of heteroleptic iridium complexes as the photosensitizer.[17] As is the case with ruthenium chromophores, utilizing iridium complexes as photosensitizers leads to a significant increase in cost for the AP system. Although this system generated over 9000 TON with respect to the iridium photosensitizers, the cobalt catalyst decomposed quickly resulting in less than 100 TON with respect to catalyst.[17]

Although there have been many reported Ni and Co catalysts for hydrogen generation in homogeneous AP systems, there has been little research reported on iron catalysts. Because Fe is the most Earth-abundant transition metal, the potential cost of Fe-based catalysts is relatively low, provided ligands can be synthesized from inexpensive precursors. Our research group has recently reported a family of iron polypyridyl catalysts that show high activity for photocatalytic hydrogen evolution from aqueous mixtures (Figure 1.5).[18]

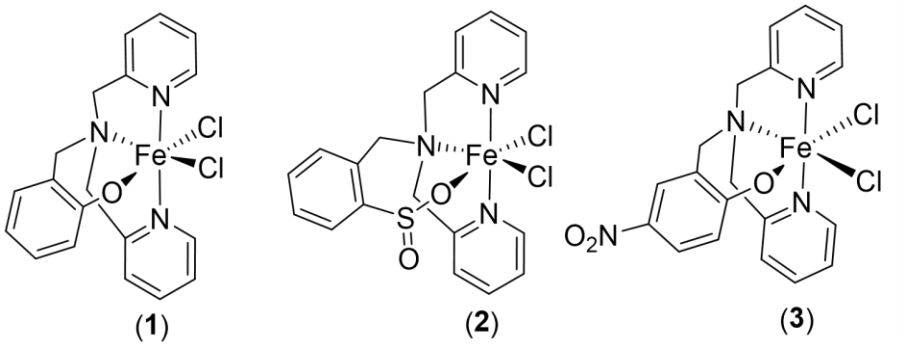

Figure 1.5. Iron polypyridyl complexes for photocatalytic hydrogen generation from aqueous mixtures.[18]

In this system, the iron polypyridyl catalyst was combined with fluorescein and triethylamine in 1:1 ethanol:water mixtures. In utilizing fluorescein as the photosensitizer, rather than a ruthenium or iridium chromophore, the cost of the system is lowered as it is a true noble-metal-free system. The most active photocatalyst was found to be the parent catalyst, $[FeCl_2(L)]$ (1), reaching 2100 TON after 24 hours of irradiation.[18] It was also reported that these catalysts were capable of generating hydrogen from aqueous mixtures containing local lake water.[18] This result, along with the use of inexpensive catalyst and photosensitizer components, provides promise for the large-scale application of the AP system.

Metal Oxide Semiconductors in Heterogeneous AP Systems

Although highly active homogeneous systems for photocatalytic hydrogen generation have been reported, these systems are limited by the effects of diffusion. In order to overcome this limitation, heterogeneous systems must be developed. One method that has been examined for heterogeneous AP systems is the incorporation of metal oxide semiconductors. These materials are of great interest because of their low cost, wide availability, and charge separation properties.[6] In addition, inorganic semiconductors are typically photochemically stable, providing increased durability to the system.[6] Metal oxide semiconductors contain a conduction band and a valence band separated by a void energy region with no energy levels.[19] When a photon of energy greater than or equal to the band gap energy of the semiconductor is absorbed, an electron-hole pair is

generated. The electron, which is promoted to the conduction band, can then migrate to the semiconductor surface, while the hole, located in the valence band, can act as an oxidant by accepting an electron.[19,20] Charge transfer of the excited electron can also occur to a species adsorbed onto the semiconductor surface.[19]

In order for metal oxide semiconductors to be incorporated into AP systems they must provide the oxidizing and/or reducing potentials necessary to split water.[6] This means that the potential of the conduction band must be less than the potential of the H^+/H_2 couple for protons to be reduced by the generated electron. Regarding the oxidative side of AP, the potential of the valence band must be greater than the potential of the O_2/H_2O couple in order for water oxidation to occur.[19,20,21] If both of these criteria are not met, such as with narrow band gap semiconductors, then the semiconductor must be combined with another semiconductor in a full AP system (Figure 1.6).[19] As a result, large band gap metal oxide semiconductors (band gap >3 eV) such as titanium dioxide (TiO_2) and strontium titanate ($SrTiO_3$) have been most often considered for AP systems. The most significant issue with the incorporation of large band gap metal oxide semiconductors is that they typically only absorb UV light, due to the high band gap energy (the amount of energy needed to promote an electron from the valence to conduction band).[6] This is a significant issue in the development of AP systems as light in the UV region constitutes less than 10% of the overall sunlight that reaches Earth.[19]

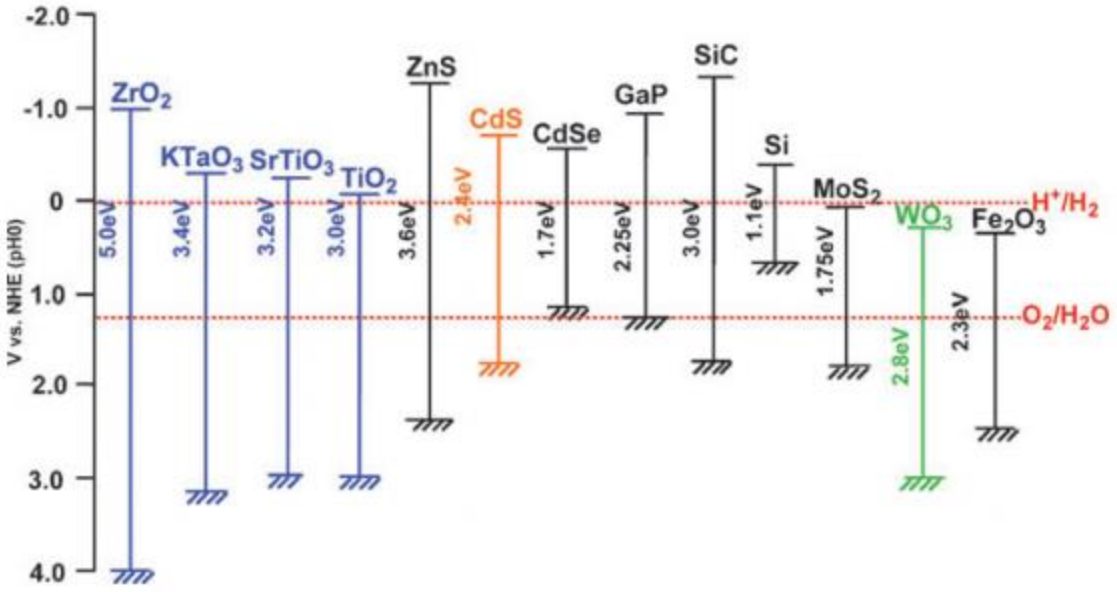

Figure 1.6. Electronic band structure of inorganic semiconductor materials as related to the redox potentials of water splitting.[22]

One method that has been investigated to address the absorption of visible light by large band gap metal oxide semiconductors is to incorporate surface photosensitization.[19] Through photosensitization, the wavelength range of light absorbed by the AP system can be significantly enhanced. Often this is accomplished by the incorporation of a chromophore on the surface of the metal oxide semiconductor. Chromophores are molecules that efficiently absorb visible light to generate an excited state. The excited state of the chromophore can then donate an electron to the conduction band of the semiconductor through charge transfer, provided the reduction potential of the excited state of the chromophore is greater than that of the conduction band of the semiconductor.[18] If charge recombination within the semiconductor is sufficiently slow, the electron can then be transferred from the conduction band to a species adsorbed on the

semiconductor surface. In many photocatalytic hydrogen generation systems ruthenium or iridium chromophores have been utilized for photosensitization. Unfortunately, the incorporation of noble metals leads to the high cost of these chromophores limiting the large-scale viability of these systems. Ideally an AP system will incorporate organic chromophores that are inexpensive and environmentally benign while also increasing the absorption of visible light within the system.

Although AP systems containing metal oxide semiconductors have been widely studied, the efficiency of the system is heavily impacted by the rate of charge recombination within the semiconductor and on the surface.[6] Fast charge recombination within the semiconductor results in decreased efficiency of solar energy conversion within the system. One method for increasing the energy conversion efficiency of the system is to add a catalyst to the metal oxide semiconductor. The catalyst can take the form of metals, dopants within the semiconductor, the addition of different semiconductors, or electrocatalysts linked to the semiconductor surface.[6,19] By incorporating a catalyst, the rate of reactions taking place at the semiconductor surface is accelerated, promoting charge transfer before charge recombination within the semiconductor can occur. For the reductive side of AP, this is accomplished by the catalyst accepting free electrons from the conduction band of the semiconductor and driving the reduction of protons on the semiconductor surface.[6]

Development of Heterogeneous AP Systems

Recently, multiple systems for heterogeneous photocatalytic hydrogen generation incorporating molecular catalysts immobilized on semiconductor surfaces have been reported. In 2011, Reisner and coworkers successfully developed a system for photocatalytic H_2 evolution from aqueous solution that incorporated a molecular cobalt complex immobilized on TiO_2.[23] In order to immobilize the catalyst on the semiconductor surface, the group functionalized a cobaloxime compound with a phosphonate anchoring group. The group then added ruthenium(II) (2,2'-bipyridine)$_2$(2,2'-bipyridine-4,4'-diylbis(phosphonic acid) bromide, [RuP]Br_2, to the catalyst-modified TiO_2 to act as a photosensitizer, again utilizing a phosphonic acid anchoring group to immobilize the molecule on the semiconductor.[23] The modified TiO_2 nanoparticles were stirred in aqueous solution in the presence of a sacrificial donor (triethanolamine) and irradiated with visible light resulting in photocatalytic H_2 generation. However, the stability of this system was not high, as the rate of H_2 evolution began to decrease after only two hours of irradiation.[23] Hydrogen generation from the system ceased completely after eight hours of irradiation resulting in a TON of only 53.[23]

Fan and coworkers have also successfully synthesized molecular cobalt catalysts for photocatalytic hydrogen evolution.[24] The most active catalyst was investigated in both homogeneous and heterogeneous systems that included Eosin Y as a photosensitizer and triethylamine as a sacrificial electron donor. Fan et al. found that hydrogen generation was significantly greater in the heterogeneous system, which utilized a carboxylic acid anchoring group to

immobilize the catalyst on TiO_2 nanoparticles.[24] At optimal conditions the heterogeneous system was found to reach 90 TON after six hours of irradiation.[24] This system is particularly noteworthy because the incorporation of Eosin Y as the photosensitizer, rather than a noble metal-based chromophore, significantly lowers the cost of the system.[24]

As is the case with homogeneous AP systems, few heterogeneous systems incorporating molecular iron complexes have been reported for photocatalytic hydrogen generation. The work presented in this thesis aims to demonstrate the immobilization of an iron polypyridyl catalyst on the surface of large band gap metal oxide semiconductors through a phosphonic acid anchoring group. The goals of this research were to demonstrate that the bond between the catalyst and semiconductor nanoparticles is durable and robust. This would allow for the catalyst-sensitized nanoparticles, along with a photosensitizer and sacrificial electron donor, to be incorporated into a heterogeneous AP system for H_2 generation from aqueous solutions. After establishing the immobilization of the catalyst on the semiconductor surface, this research sought to optimize the AP system for photocatalytic hydrogen generation.

References

1. Chen, N. Y. *Chem. Innov.* **2001,** *31* (1), 14-20.
2. International Energy Outlook 2017. U.S. Energy Administration. https://www.eia.gov/outlooks/ieo/exec_summ.php (accessed March 11, 2018).
3. Resources to Reserves 2013. International Energy Association. https://www.iea.org/publications/freepublications/publication/Resources2013.pdf (accessed March 12, 2018).
4. BP Energy Outlook. British Petroleum. https://www.bp.com/en/global/corporate/energy-economics/energy-outlook.html (accessed March 26, 2018).
5. Pisupati, S. Energy Reserves. Penn State College of Earth and Mineral Sciences. **2017**. https://www.e-education.psu.edu/egee102/node/1932 (accessed March 18, 2018).
6. Barber, J.; Tran, P. D. From natural to artificial photosynthesis. *J. R. Soc. Inter.* **2013**.
7. Le Treut, H., R. Somerville, U. Cubasch, Y. Ding, C. Mauritzen, A. Mokssit, T. Peterson and M. Prather, 2007: Historical Overview of Climate Change. In: Climate Change 2007: The Physical Science Basis. Contribution of Working Group I to the Fourth Assessment Report of the Intergovernmental Panel on Climate Change [Solomon, S., D. Qin, M. Manning, Z. Chen, M. Marquis, K.B. Averyt, M. Tignor and H.L. Miller (eds.)]. Cambridge University Press, Cambridge, United Kingdom and New York, NY, USA.
8. Dunn, R. J. H.; Hurst, D. F.; Gobron, N.; Willett, K. M. Eds., 2017: Global Climate [in: State of the Climate in 2016]. *Bull. Amer. Meteor. Soc.*, **98** (8), S5-S62, doi:10.1175/2017BAMSStateoftheClimate.1.
9. Dahlman, L. Climate Change: Global Temperature. National Oceanic and Atmospheric Administration. **2017**. https://www.climate.gov/news-features/understanding-climate/climate-change-global-temperature (accessed March 26, 2018).
10. P. Du and R. Eisenberg. Catalysts made of earth-abundant elements (Co, Ni, Fe) for water splitting: Recent progress and future challenges. *Energy Environ. Sci.* **2012**, *5*, 6012-6021.
11. A. J. Esswein and D. G. Nocera. Hydrogen production by molecular photocatalysis. *Chem. Rev.* **2007**, *107*, 4022-4047.
12. W. T. Eckenhoff and R. Eisenberg. Molecular systems for light driven hydrogen production. *Dalton Trans.* **2012**, *41*, 13004-13021.
13. Han, Z.; McNamara, W. R.; Eum, M-S.; Holland, P. L.; Eisenberg, R. A nickel thiolate catalyst for the long-lived photocatalytic production of hydrogen in a noble-metal free system. *Ang. Chem. Int. Ed.* **2012**, *51* (7), 1667-1670.
14. McLaughlin, M. P.; McCormick, T. M.; Eisenberg, R.; Holland, P. L. A stable molecular nickel catalyst for the homogeneous photogeneration of hydrogen in aqueous solution. *Chem Commun.* **2011**, *47*, 7989-7991.

15. Du, P.; Schneider, J.; Luo, G.; Brennessel, W. W.; Eisenberg, R. Visible light-driven hydrogen production from aqueous protons catalyzed by molecular cobaloxime catalysts. *Inorg. Chem.* **2009**, *48*, 4952-4962.
16. McNamara, W. R.; Han, Z.; Yin, C-J.; Brennessel, W. W.; Holland, P. L.; Eisenberg, R. Cobalt-dithiolene complexes for the photocatalytic and electrocatalytic reduction of protons in aqueous solutions. *PNAS*. **2012**, *109* (39), 15594-15599.
17. Goldsmith, J. I.; Hudson, W. R.; Lowry, M. S.; Anderson, T. H.; Bernhard, S. Discovery and high-throughput screening of heteroleptic iridium complexes for photoinduced hydrogen production. *J. Am. Chem. Soc.* **2005**, *127*, 7502-7510.
18. Hartley, C. L.; DiRisio, R. J.; Screen, M. E.; Mayer, K. J.; McNamara, W. R. Iron polypyridyl complexes for photocatalytic hydrogen generation. *Inorg. Chem.* **2016**, *55*, 8865-8870.
19. Linsebigler, A. L.; Lu, G.; Yates, J. T. Photocatalysis on TiO_2 surfaces: Principles, mechanisms, and selected results. *Chem. Rev.* **1995**, *95*, 735-758.
20. Hermann, J. Heterogeneous photocatalysis: fundamentals and applications to the removal of various types of aqueous pollutants. *Catalysis Today*. **1999**, *53*, 115-129.
21. A. Mills and S. Le Hunte. An overview of semiconductor photocatalysis. *J. Photochemistry and Photobiology A: Chemistry*. **1997**, *108* (1), 1-35.
22. A. Kudo and Y. Miseki. Heterogeneous photocatalyst materials for water splitting. *Chem. Soc. Rev.* **2009**, *38*, 253-278.
23. E. Reisner and F. Lakadamyali. Photocatalytic H_2 evolution from neutral water with a molecular cobalt catalyst on a dye-sensitised TiO_2 nanoparticle. *Chem. Commun.* **2011**, *47*, 1695-1697.
24. Yin, M.; Ma, S.; Wu, C.; Fan, Y. A noble-metal-free photcatalytic hydrogen production system based on cobalt (III) complex and eosin Y-sensitized TiO_2. *RSC Adv.* **2015**, *5*, 1852-1858.

Chapter 2. Immobilization of [$FeCl_2$(L-PO_3H_2)] on Semiconductors

Introduction

Immobilization of the iron polypyridyl catalyst on the surface of metal oxide semiconductors was desirable for multiple reasons. A primary benefit of immobilization of the catalyst is that moving from a homogeneous system, where catalyst is dissolved in solution, to a heterogeneous system allows us to overcome the issue of diffusion within the reaction mixture. Immobilization of the proton reduction catalyst on semiconductor nanoparticles also allows us the opportunity to recycle and reuse the catalyst-sensitized nanoparticles. The durability and stability of the catalyst-sensitized nanoparticles, which can be attributed to the photostability of inorganic semiconductor materials such as $SrTiO_3$ and TiO_2, makes recycling the catalyst significantly more plausible than in the homogeneous system. Through the binding of the Fe catalyst to the surface of the semiconductor materials we are able to take advantage of increased stability while maintaining the proton reduction activity of the previously reported Fe catalysts.

In order for our AP system to be successful and durable, the bond linking the Fe catalyst to the metal oxide semiconductor must be stable under various conditions. Although many organic functional groups have been investigated as anchoring groups on metal oxide semiconductors such as $SrTiO_3$ and TiO_2, the most commonly utilized anchoring groups are silanes, carboxylates, and phosphonic acids.[1] Silanes are not seen as good candidates for anchoring groups in AP systems as it has been shown that organosilyated metal oxides are

susceptible to hydrolysis.[1] Previous research in our lab has investigated carboxylates as a possible anchoring group to immobilize the Fe catalyst on TiO_2, but it was found that the bond to TiO_2 was not water stable. This is supported by additional research that has found that the bonding of carboxylates to metal oxide surfaces is relatively weak.[1] Because of these issues, phosphonic acids provide the most promise as anchoring groups in AP systems. One benefit of using phosphonic acids as anchoring groups on metal oxide semiconductors such as TiO_2 is the strength of P-O-Ti bonds. Additionally, it has been shown that the surface of TiO_2 can be modified by phosphonic acids in both water and organic solvents.[1] This is extremely important in our case as large-scale AP systems will need to be deployed in water for cost-effective H_2 generation.

In theory, phosphonic acid functional groups can bind to metal oxide semiconductor surfaces in mono-, bi-, and tridentate fashions (Figure 2.1). Recent research has focused on the binding modes of phosphonic acid derivatives on TiO_2 anatase surfaces.[1] This research showed multiple binding modes of the phosphonic acid derivatives on both TiO_2 anatase (101) and (001). The binding of phosphonic acid derivatives to the surface of TiO_2 anatase (101) was found to occur in both monodentate and bidentate fashions, with the singly deprotonated bidentate mode being slightly more stable.[1] In contrast, the phosphonic acid derivatives were found to bind to TiO_2 anatase (001) in a bidentate and tridentate fashion with the doubly deprotonated bidentate binding mode showing slightly greater stability.[1]

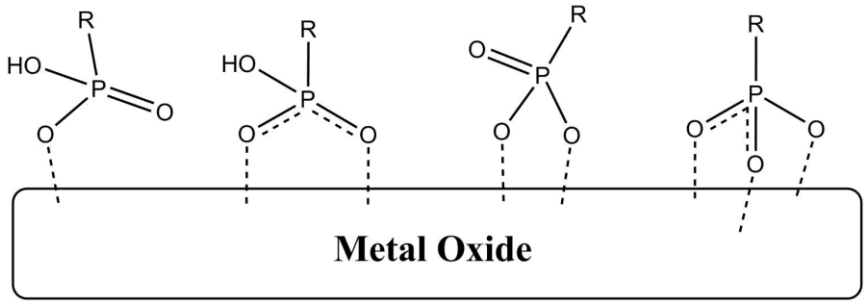

Figure 2.1. Binding modes of phosphonic acids on metal oxide semiconductor surfaces.

Recently, our group has successfully synthesized a phosphonic acid-functionalized polypyridyl ligand, L-PO_3H_2 (Figure 2.2). This ligand mirrors the ligands incorporated into the previously reported hydrogen generation catalysts.[3,4,5]

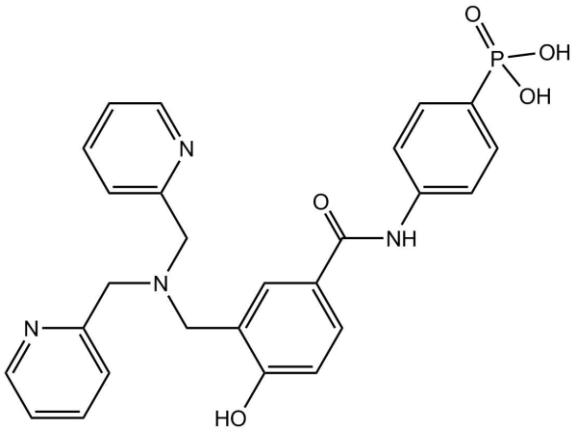

Figure 2.2. Phosphonic acid functionalized polypyridyl ligand, (L-PO_3H_2).

One drawback to the strong binding that occurs between phosphonic acids and metal centers is that we are unable to isolate the fully assembled

phosphonic acid derivative of the Fe polypyridyl catalyst, [$FeCl_2$(L-PO_3H_2)]. When L-PO_3H_2 is exposed to iron, the phosphonic acid group chelates to the open site of the iron center, forming an insoluble polymeric material rather than the active polypyridyl catalyst. To circumvent this issue, the phosphonic acid group of the ligand must be protected prior to complexation with iron. This was accomplished by binding the ligand to the surface of the semiconductor nanoparticles prior to introducing Fe (Figure 2.3). The phosphonic acid group of the ligand preferentially binds to the metal oxide semiconductor, promoting binding of the polypyridyl ligand to Fe in the manner observed in the previously reported Fe catalysts.

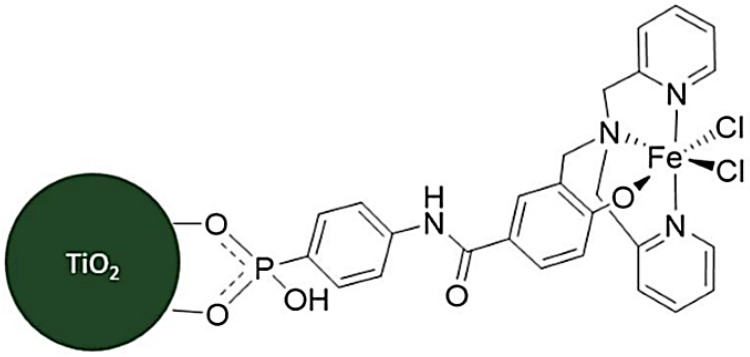

Figure 2.3. Phosphonic acid functionalized iron polypyridyl catalyst, [$FeCl_2$(L-PO_3H_2)], immobilized on TiO_2 nanoparticle

The research reported in this chapter describes the immobilization of the iron polypyridyl catalyst on different metal oxide semiconductor surfaces through a phosphonic acid functional group. [$FeCl_2$(L-PO_3H_2)] was assembled on the surface of semiconductor nanoparticles through both a thin film and centrifuge

procedure. The binding of both (L-PO_3H_2) and [$FeCl_2$(L-PO_3H_2)] was investigated using diffuse reflectance UV-Vis spectroscopy and powder ATR-FTIR spectroscopy. Diffuse Reflectance UV-Vis was also used to examine the durability of the bond between [$FeCl_2$(L-PO_3H_2)] and the semiconductor nanoparticles when exposed to the conditions of our photochemical system. The aggregation of the organic chromophore fluorescein on the surface of semiconductor nanoparticles was investigated through diffuse reflectance UV-Vis and powder ATR-FTIR as well.

Experimental Procedure

Materials and Methods

$SrTiO_3$ nanopowder (diameter = 25 nm) was obtained from Alfa Aesar. P25 TiO_2 powder was obtained from Acros Organics. Zirconia (diameter = 20 nm) was purchased from Sigma Aldrich. Triethylamine (99%) and triethanolamine (97%) were used as received and obtained from Acros Organics. Fluorescein and Eosin Y were also used as received and obtained from Acros Organics. All other reagents were purchased from Fisher Scientific and used without further purification.

Instrumentation

^{1}H and ^{13}C NMR spectra were obtained using an Agilent 400MR DD2 spectrometer operating in the pulse Fourier transform mode. Chemical shifts are reported in ppm with the residual solvent as an internal reference. Mass spectrometry was carried out using positive electrospray ionization on a Bruker 12 Tesla APEX-Qe FTICR-MS with an Apollo II ion source. All UV-Vis analysis was performed using an Agilent Cary 60 Spectrophotometer. IR analysis was performed using a Shimadzu IRTracer-100 FTIR with a MIRacle 10 Single Reflection ATR Accessory.

Preparation of Semiconductor Thin Films

Metal oxide semiconductor thin films were prepared through the addition of semiconductor nanoparticles and deionized water to a sample vial in a ratio of 4.0 g : 7.0 mL. This mixture was capped and sealed with Parafilm, then stirred for at least four hours to form a slurry. The slurry was then transferred to one side of glass microscope slides using a Pasteur pipette. A thin film of the semiconductor slurry was spread over the microscope slides using the doctor-blading technique with a clean razor blade to give a thin, even layer.[6] The resulting films were then cured in a muffle furnace at 150 °C for two hours.

Immobilization of [$FeCl_2$(L-PO_3H_2)] on Semiconductor Thin Films

Immobilization of [$FeCl_2$(L-PO_3H_2)] on metal oxide semiconductor thin films was a two-step process. First, a metal oxide semiconductor thin film was soaked in 8 x 10^{-7} moles of L-PO_3H_2, with excess methanol to completely submerge the thin film, in a petri dish wrapped in aluminum foil for 30 minutes. A watch glass was used to cover the petri dish and aluminum foil covers were used to prevent light contamination. After soaking, the L-PO_3H_2-sensitized semiconductor thin film was removed from the petri dish and rinsed with methanol, water, and dichloromethane. The petri dish was emptied and rinsed with water and methanol. The thin film was then returned to the petri dish and soaked in 8 x 10^{-7} moles of iron(III) chloride, with excess methanol to completely submerge the thin film, for 30 minutes. A watch glass was again used to cover the petri dish and aluminum foil covers were added to prevent light contamination. After soaking in

$FeCl_3$, the metal oxide semiconductor thin film had a fairly strong purple color, indicating that the catalyst had been complexed on the surface of the thin film. The thin film was removed from the petri dish and rinsed with methanol, water, and dichloromethane. The [$FeCl_2$(L-PO_3H_2)]-sensitized thin film was then allowed to dry in the dark prior to use.

Immobilization of [$FeCl_2$(L-PO_3H_2)] on Semiconductors via Centrifuge

Immobilization of the [$FeCl_2$(L-PO_3H_2)] on metal oxide semiconductor nanoparticles via the centrifuge method was also a two-step process. A measured amount of metal oxide semiconductor nanoparticles with excess L-PO_3H_2 in solution (1.0×10^{-7} moles ligand in methanol per 5 mg semiconductor nanoparticles) was added to a sample vial. Excess methanol was added to the sample vial to bring the total volume to 5.0 mL. The sample vial was capped and sealed with Parafilm and the mixture was stirred for one hour. After stirring, the mixture was divided into microcentrifuge tubes and centrifuged at 13,400 rpm for 15 minutes. The supernatant was removed, followed by the addition of fresh methanol to the microcentrifuge tubes to rinse the L-PO_3H_2 -sensitized nanoparticles. The mixtures were stirred and sonicated prior to being centrifuged again at 13,400 rpm for three minutes. The previously described wash process involving the three-minute centrifugation of the mixtures was completed a total of four times. Following the final centrifugation of the mixtures, the supernatant was removed and the L-PO_3H_2 -sensitized nanoparticles were transferred to a clean sample vial. Excess iron(III) chloride solution (1.0×10^{-7} moles $FeCl_3$ in methanol

per 5 mg semiconductor nanoparticles) was added to a sample vial along with excess methanol to bring the total volume to 5.0 mL. The sample vial was capped and sealed with Parafilm and the mixture was stirred for one hour. While stirring, it was observed that the mixture underwent a color change from white to pale purple indicating complexation of the catalyst on the semiconductor nanoparticles' surface. After stirring, the mixture was divided into clean microcentrifuge tubes and subjected to the identical centrifugation and washing procedure as previously outlined with the L-PO3H_2-sensitized nanoparticles. Following the final centrifugation of the mixtures, the supernatant was removed and the [$FeCl_2$(L-PO_3H_2)]-sensitized nanoparticles were allowed to dry overnight in the dark.

Results and Discussion

Immobilization of L-PO_3H_2 and [$FeCl_2$(L-PO_3H_2)] on Semiconductors

In order to confirm that L-PO_3H_2 and [$FeCl_2$(L-PO_3H_2)] were successfully immobilized on the metal oxide semiconductor nanoparticles, diffuse reflectance UV-Vis spectrophotometry was used. $SrTiO_3$ and TiO_2 thin films were prepared on glass microscope slides and then sensitized with L-PO_3H_2. Fe(III) chloride was then introduced to the L-PO_3H_2-sensitized thin films to form the fully assembled [$FeCl_2$(L-PO_3H_2)] on the surface of the semiconductor nanoparticles. Diffuse reflectance spectra were recorded of the bare semiconductor thin films, L-PO_3H_2-sensitized semiconductor thin films, and [$FeCl_2$(L-PO_3H_2)]-sensitized thin films (Figure 2.4).

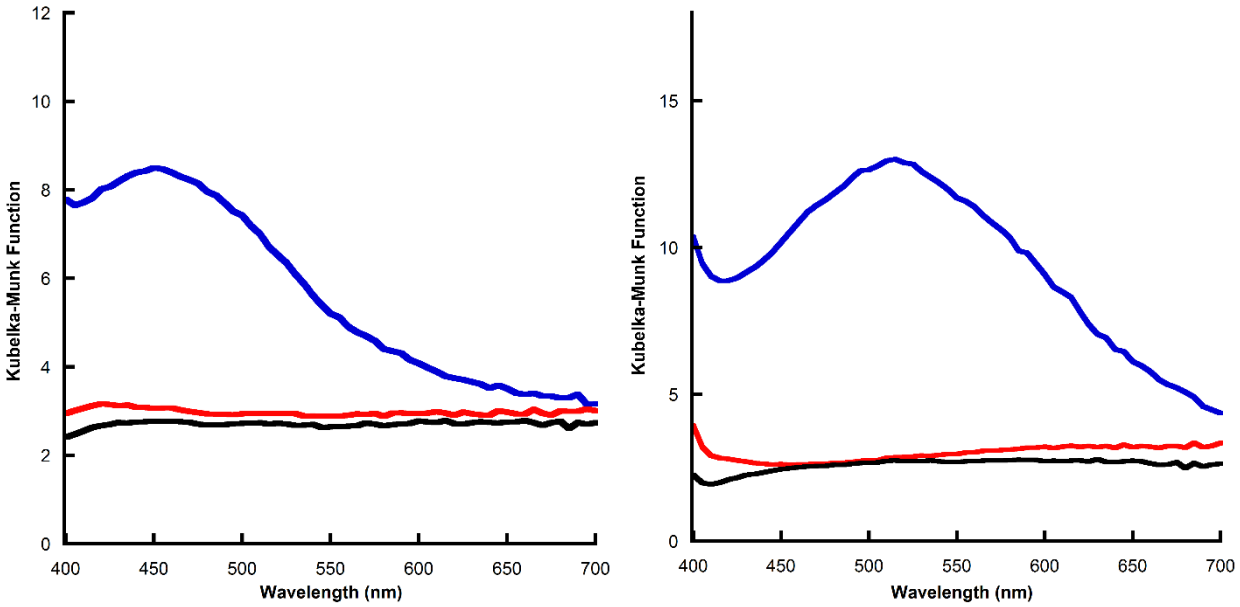

Figure 2.4. *Left:* Diffuse Reflectance UV-Vis spectra of thin film of bare $SrTiO_3$ (black), L-PO_3H_2-$SrTiO_3$ (red), and [$FeCl_2$(L-PO_3H_2)]-$SrTiO_3$ (blue). *Right:* Diffuse Reflectance UV-Vis spectra of thin film of bare TiO_2 (black), L-PO_3H_2-TiO_2 (red), and [$FeCl_2$(L-PO_3H_2)]-TiO_2 (blue).

Analysis of the diffuse reflectance UV-Vis spectra indicated that the L-PO_3H_2-sensitized semiconductor thin films have a slightly greater absorbance across the visible spectrum than the bare metal oxide semiconductor nanoparticles. Assembly of the catalyst on the surface of the semiconductor nanoparticles was indicated by a significant increase in absorbance across much of the visible spectrum. This change was also observed visually, as the color of the semiconductor thin films changed from white to purple upon assembly of [$FeCl_2$(L-PO_3H_2)] on the semiconductor surface. Immobilization of L-PO_3H_2 and [$FeCl_2$(L-PO_3H_2)] on the surface of $SrTiO_3$ and TiO_2 nanoparticles was also confirmed through powder ATR-FTIR. Analysis of the spectra of ligand and catalyst-sensitized nanoparticles indicated characteristic phosphonic acid stretching at approximately 2550 cm^{-1} (see Appendix A). Diffuse reflectance spectra were also collected for bare ZrO_2 thin films, L-PO_3H_2-ZrO_2, and [$FeCl_2$(L-PO_3H_2)]-ZrO_2 for comparison to the spectra of $SrTiO_3$ and TiO_2 (see Appendix A). Zirconia is of interest as a control material because it is also a large-band gap metal oxide semiconductor. However, the reduction potential of the conduction band of ZrO_2 is too negative to accept electrons from the excited state of many rhodamine dyes such as fluorescein and Eosin Y.[8] This prevents injection of electrons from the photosensitizer into the semiconductor, thus preventing charge transfer.[9]

The maximum absorbance of the diffuse reflectance spectrum of [$FeCl_2$(L-PO_3H_2)]-$SrTiO_3$ nanoparticles was determined to be at 475 nm. Interestingly, the maximum absorbance of [$FeCl_2$(L-PO_3H_2)]-TiO_2 nanoparticles was determined to

be at a lower energy, 515 nm. This indicated that there was likely a difference in the environment at the surface of the different metal oxide semiconductor nanoparticles. We theorized that the pH at the surface of the semiconductor nanoparticles may be slightly different, causing the observed change in the spectra.

In order to better understand the difference in the diffuse reflectance UV-Vis spectra of $[FeCl_2(L\text{-}PO_3H_2)]$-$SrTiO_3$ and $[FeCl_2(L\text{-}PO_3H_2)]$-$TiO_2$, we investigated the effect that changes in pH may have on the UV-Vis spectrum of the parent catalyst, $[FeCl_2(L)]$. In this study, we analyzed the parent complex, $[FeCl_2(L)]$, in 1:1 mixtures of ethanol:water via UV-Vis spectrophotometry (Figure 2.5). The pH of the solvent mixtures was adjusted with 1 M HCl and 1 M NaOH prior to analysis.

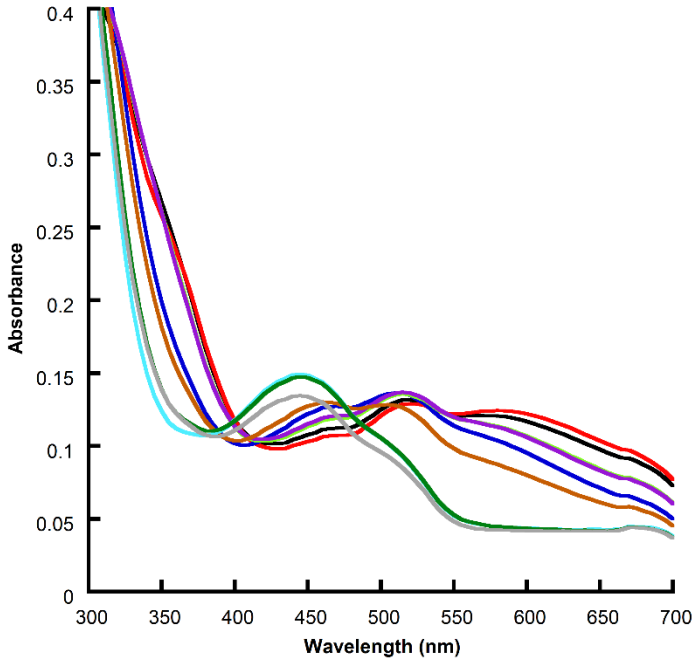

Figure 2.5. UV-Vis spectra of 6 x 10^{-5} M $[FeCl_2(L)]$ in 1:1 ethanol:water adjusted to pH 4 (black), pH 5 (red), pH 6 (dark blue), pH 7 (light green), pH 8 (purple), pH 9 (brown), pH 10 (light blue), pH 11 (dark green), and pH 12 (gray).

In comparing the UV-Vis spectra of [$FeCl_2$(L)] in solution at different pH values, a shift in the wavelength of maximum absorbance was observed as the pH of the solution changed. At lower pH (4-8), the wavelength of maximum absorbance was observed to be approximately 515 nm. At significantly basic pH (10-12), the wavelength of maximum absorbance of [$FeCl_2$(L)] was observed to be approximately 445 nm. The observed shift in the wavelength of maximum absorbance mirrors the difference in the maximum absorbance of the diffuse reflectance spectra of [$FeCl_2$(L-PO_3H_2)]-TiO_2 and [$FeCl_2$(L-PO_3H_2)]-$SrTiO_3$. The similarities between the UV-Vis spectra of [$FeCl_2$(L)] and the diffuse reflectance spectra of [$FeCl_2$(L-PO_3H_2)]-sensitized nanoparticles indicates that there is a difference in pH at the surface of the two metal oxide semiconductors. Based on these results, the pH at the surface of $SrTiO_3$ nanoparticles is likely in the range of 9-10, while the pH at the surface of TiO_2 nanoparticles is more acidic, likely in the range of 5-8. Further studies utilizing diffuse reflectance UV-Vis spectrophotometry determined that the shift in maximum absorbance can be prompted by soaking [$FeCl_2$(L-PO_3H_2)]-sensitized semiconductor thin films in solutions at different pH values. Altering the pH of the environment at the semiconductor surface also indicated that the observed absorbance shift was reversible (see Appendix A).

After establishing that [$FeCl_2$(L-PO_3H_2)] was successfully immobilized on the metal oxide semiconductor nanoparticles, it was important to confirm that the binding of [$FeCl_2$(L-PO_3H_2)] to the surface of the nanoparticles was stable when exposed to our photochemistry conditions, which require the presence of a

sacrificial electron donor in aqueous mixtures. To investigate this, [$FeCl_2$(L-PO_3H_2)] was immobilized on a $SrTiO_3$ thin film in the manner previously described and analyzed by diffuse reflectance UV-Vis spectrophotometry. The thin film was then soaked in a 1:1 ethanol:water mixture containing 5% v/v triethylamine, mimicking our photochemistry conditions. The diffuse reflectance spectrum of the [$FeCl_2$(L-PO_3H_2)]-$SrTiO_3$ thin film was then collected for comparison to the previously collected [$FeCl_2$(L-PO_3H_2)]-$SrTiO_3$ spectrum (Figure 2.6).

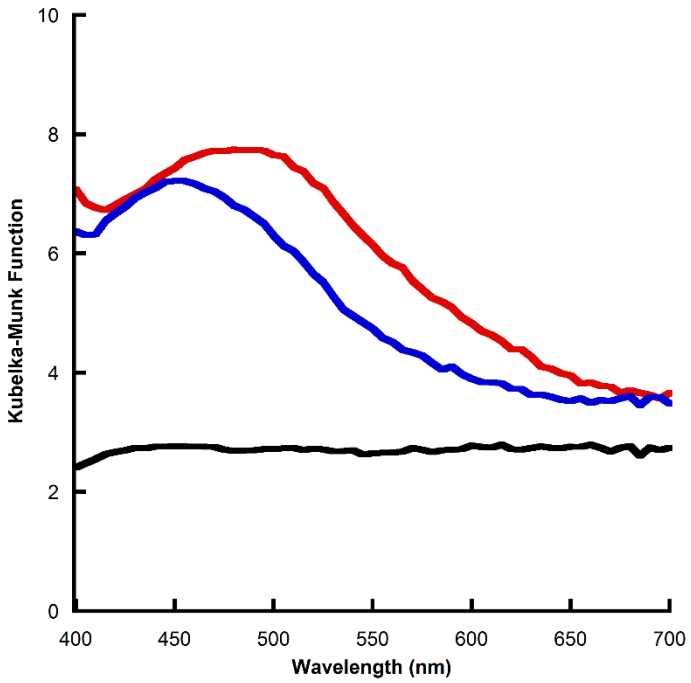

Figure 2.6. Diffuse Reflectance UV-Vis spectra of thin film of bare $SrTiO_3$ (black), [$FeCl_2$(L-PO_3H_2)]-$SrTiO_3$ (red), and [$FeCl_2$(L-PO_3H_2)]-$SrTiO_3$ after soaking in 1:1 ethanol:water with 5% v/v triethylamine (blue).

In comparing the spectra of the [$FeCl_2$(L-PO_3H_2)]-sensitized $SrTiO_3$ thin films before and after exposure to photochemistry conditions, a clear shift in the

wavelength of maximum absorbance is observed. This shift follows the previously observed trend relating the shift in maximum absorbance to shorter wavelength to an increase in pH at the semiconductor surface. The increased pH of the semiconductor surface can be attributed to the presence of the sacrificial electron donor triethylamine, which has a pKa of 10.75. The shift in absorbance may also explain the observed decrease in absorbance of $[FeCl_2(L\text{-}PO_3H_2)]$-$SrTiO_3$ from approximately 460-680 nm, after the thin film was exposed to photochemistry conditions. Another possible explanation for this decrease in absorbance is loss of catalyst from the semiconductor surface. This could occur when the $[FeCl_2(L\text{-}PO_3H_2)]$-$SrTiO_3$ thin film is submerged in the photochemistry mixture or when the thin film is rinsed with solvent after it is removed from the mixture. Despite the observed decrease in absorbance, it is clear that the immobilization of $[FeCl_2(L\text{-}PO_3H_2)]$ on the semiconductor surface is sufficiently stable when exposed to aqueous photochemistry conditions.

Sensitizing Metal Oxide Semiconductors with Fluorescein

As mentioned previously, incorporating a chromophore into AP systems allows for more efficient absorption of visible light by the system. Because of this, it was important to determine if inexpensive organic chromophores could be incorporated onto the surface of the metal oxide semiconductor nanoparticles. To investigate this, a $SrTiO_3$ thin film and a TiO_2 thin film prepared in the typical manner were soaked separately in 4.0 mM solutions of fluorescein in ethanol in the dark. Fluorescein was chosen as the chromophore because the oxidative

energy level of the excited state is more negative than the conduction band of $SrTiO_3$ and TiO_2, allowing for electron transfer from the excited state of the chromophore to the conduction band of the semiconductor.[7] After soaking, the thin films were analyzed by diffuse reflectance UV-Vis spectrophotometry (Figure 2.7).

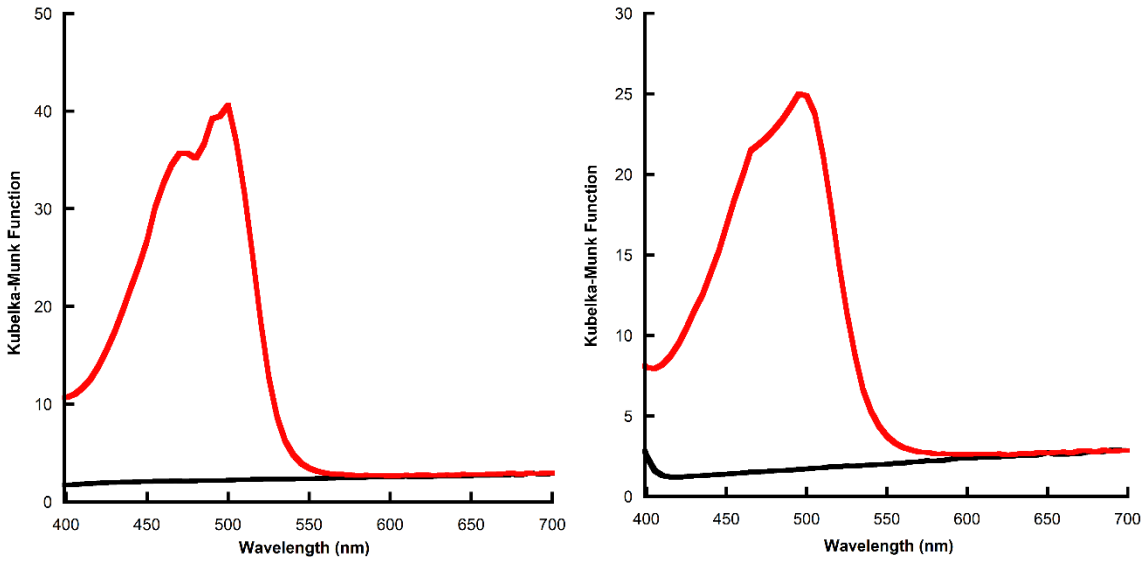

Figure 2.7. *Left:* Diffuse Reflectance UV-Vis spectra of thin film of bare $SrTiO_3$ (black) and fluorescein sensitized $SrTiO_3$ thin film (red).
Right: Diffuse Reflectance UV-Vis spectra of thin film of bare TiO_2 (black) and fluorescein sensitized TiO_2 thin film (red).

Sensitization of the metal oxide semiconductor thin films with fluorescein resulted in significantly increased absorbance in the visible light wavelength range, particularly between 400 and 525 nm. The wavelength of maximum absorbance for the fluorescein-sensitized $SrTiO_3$ nanoparticles and fluorescein-sensitized TiO_2 nanoparticles was determined to be 500 nm. Powder ATR-FTIR was also utilized to confirm the surface sensitization of $SrTiO_3$ and TiO_2 with

fluorescein (see Appendix A). It is likely that the sensitization of the semiconductor surfaces was the result of aggregation of fluorescein on the nanoparticles, rather than covalent bonding between the carboxylic acid group of the chromophore and semiconductor. As previously mentioned, the bonds between carboxylic acid groups and metal oxide semiconductors are relatively weak, while aggregation of multiple structurally similar chromophores on TiO_2 has been reported.[1,9,10] The collected diffuse reflectance spectra indicated that sensitizing the metal oxide semiconductor nanoparticles with fluorescein greatly increased visible light absorption, thus increasing the efficiency of solar energy conversion within the prospective AP system.

After confirming the immobilization of [$FeCl_2$(L-PO_3H_2)] and aggregation of fluorescein on the surface of semiconductor nanoparticles separately, it was of interest to examine the nanoparticles when the catalyst and chromophore are both present. To investigate this, a [$FeCl_2$(L-PO_3H_2)]-$SrTiO_3$ thin film prepared in the typical manner was soaked in a 1:1 mixture of ethanol:water containing 5% v/v triethylamine and 0.4 mM fluorescein. The thin film was analyzed by diffuse reflectance UV-Vis spectrophotometry both before and after soaking in the mixture (Figure 2.8).

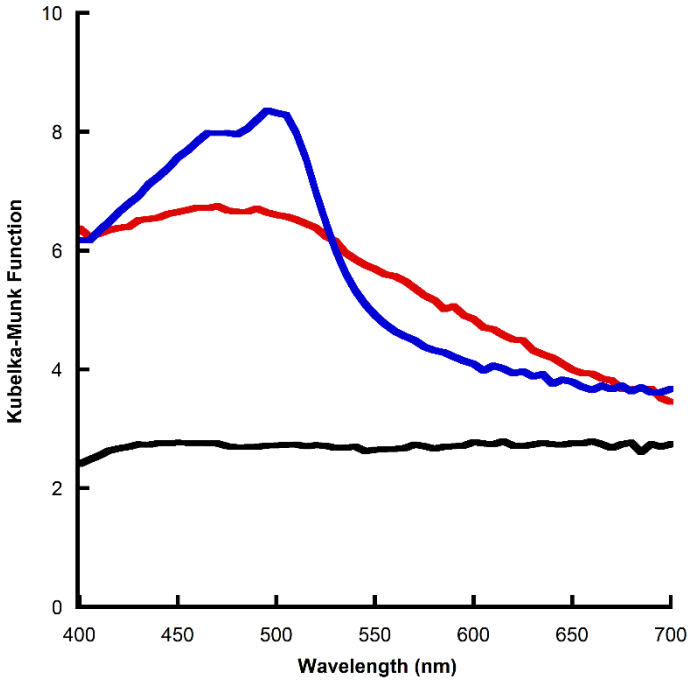

Figure 2.8. Diffuse Reflectance UV-Vis spectra of thin film of bare $SrTiO_3$ (black), $[FeCl_2(L\text{-}PO_3H_2)]$-$SrTiO_3$ (red), and $[FeCl_2(L\text{-}PO_3H_2)]$-$SrTiO_3$ after soaking in 1:1 ethanol:water with 5% v/v triethylamine and 0.4 mM fluorescein.

Exposure of the $[FeCl_2(L\text{-}PO_3H_2)]$-$SrTiO_3$ thin film to our photochemistry conditions with fluorescein present resulted in a significant increase in the absorbance from approximately 425-525 nm. This increase in absorbance can be attributed to the aggregation of fluorescein on the semiconductor surface. Importantly, this indicates that the aggregation of fluorescein on the surface of $SrTiO_3$ is not impacted by the presence of the immobilized catalyst. In addition, the results of this study further indicated that both the sensitization of the chromophore and catalyst on the semiconductor nanoparticles is stable when exposed to photochemistry conditions.

Conclusion

The research reported in this chapter demonstrates the robust and durable binding of an iron polypyridyl catalyst, [$FeCl_2$(L-PO_3H_2)], on large band gap metal oxide semiconductor nanoparticles. The bond between the phosphonic acid anchoring group and the semiconductor surface has been shown to be stable in conditions under which photochemistry studies would be conducted. In addition, this research established that there is a difference in pH at the surface of $SrTiO_3$ and TiO_2 that is reflected in the UV-Vis spectra of the [$FeCl_2$(L-PO_3H_2)]-sensitized nanoparticles. At lower pH, the wavelength of maximum absorbance of the immobilized catalyst was found to be at lower energy than the maximum absorbance at significantly basic pH. This research also established that sensitizing $SrTiO_3$ and TiO_2 nanoparticles with the organic chromophore fluorescein significantly increases the absorbance of the semiconductor material in the visible spectrum, particularly from 400-525 nm. These results suggest that the immobilization of [$FeCl_2$(L-PO_3H_2)] on $SrTiO_3$ and TiO_2 nanoparticles has significant promise for incorporation into a heterogeneous AP system for photocatalytic hydrogen generation.

References

1. Geldof, D.; Tassi, M.; Carleer, R.; Adriaensens, P.; Roevens, A.; Meynen, V.; Blockhuys, F. Binding modes of phosphonic acid derivatives adsorbed on TiO2 surfaces: Assignments of experimental IR and NMR spectra based on DFT/PBC calculations. *Surface Science*. **2017**, *655*, 31-38.
2. Brennan, B. J.; Llansola Portoles, M. J.; Liddell, P. A.; Moore, T. A.; Moore, A. L.; Gust, D. Comparison of silatrane, phosphonic acid, and carboxylic acid functional groups for attachment of porphyrin sensitizers to TiO_2 in photoelectrochemical cells. *Phys. Chem. Chem. Phys.* **2013**, *15*, 16605-16614.
3. Connor, G. P.; Mayer, K. J.; Tribble, C. S.; McNamara, W. R. Hydrogen evolution catalyzed by an iron polypyridyl complex in aqueous solutions. *Inorg. Chem.* **2014**, *53* (11), 5408-5410.
4. Cavell, A. C.; Hartley, C. L.; Liu, D.; Tribble, C. S.; McNamara, W. R. Sulfinato iron (III) complex for electrocatalytic proton reduction. *Inorg. Chem.* **2015**, *54* (7), 3325-3330.
5. Hartley, C. L.; DiRisio, R. J.; Chang, T. Y.; Zhang, W.; McNamara, W. R. Electrocatalytic hydrogen evolution by an iron complex containing a nitro-functionalized polypyridyl ligand. *Polyhedron*, **2016**, *114*, 133-137.
6. McNamara, W. R.; Snoeberger III, R. C.; Li, G.; Schleicher, J. M.; Cady, C. W.; Poyatos, M.; Schmuttenmaer, C. A.; Crabtree, R. H.; Brudvig, G. W.; Batista, V. S. Acetylacetonate anchors for robust functionalization of TiO_2 nanoparticles with Mn(II) – terpyridine complexes. *J. Am. Chem. Soc.* **2008**, *130* (43), 14329-14338.
7. Linsebigler, A. L.; Lu, G.; Yates, J. T. Photocatalysis on TiO_2 surfaces: Principles, mechanisms, and selected results. *Chem. Rev.* **1995**, *95*, 735-758.
8. A. Kudo and Y. Miseki. Heterogeneous photocatalyst materials for water splitting. *Chem. Soc. Rev.* **2009**, *38*, 253-278.
9. Cassidy, J. P.; Tan, J. A.; Wustholz, K. L. Probing the aggregation and photodegradation of rhodamine dyes on TiO_2. *J. Phys. Chem. C*, **2017**, *121* (29), 15610-15618.
10. Mulher, K. R.; Detty, M. R.; Watson, D. F. Aggregation-induced increase of the quantum yield of electron injection from chalcogenorhodamine dyes to TiO_2. *J. Phys. Chem. C*, **2011**, *115* (13), 6010-6018.

Appendix A

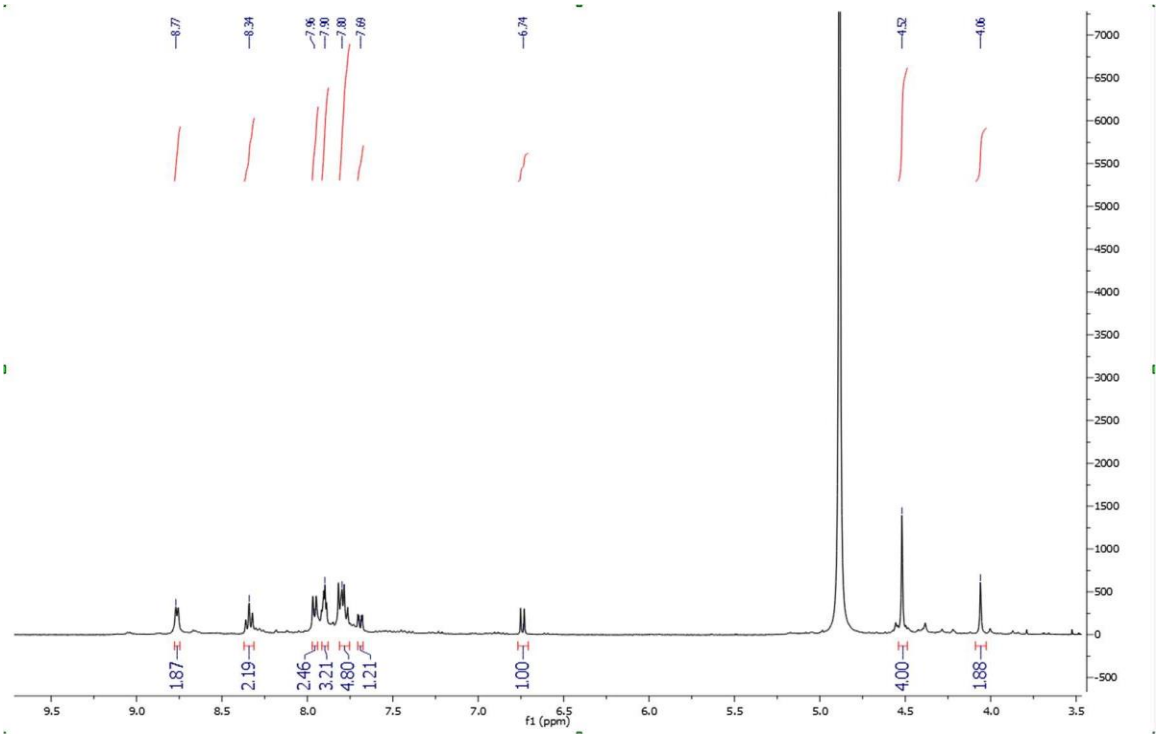

Figure A.1. ^{1}H NMR spectrum of L-PO_3H_2 with integrations in blue.

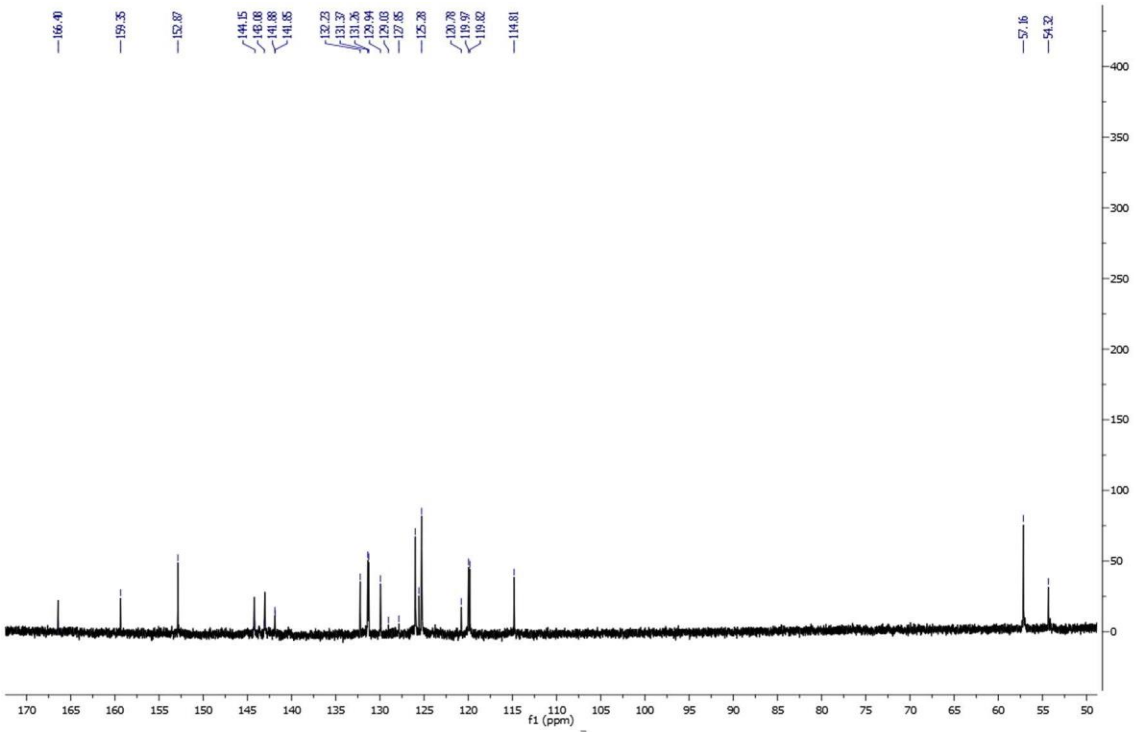

Figure A.2. ^{13}C NMR spectrum of L-PO_3H_2.

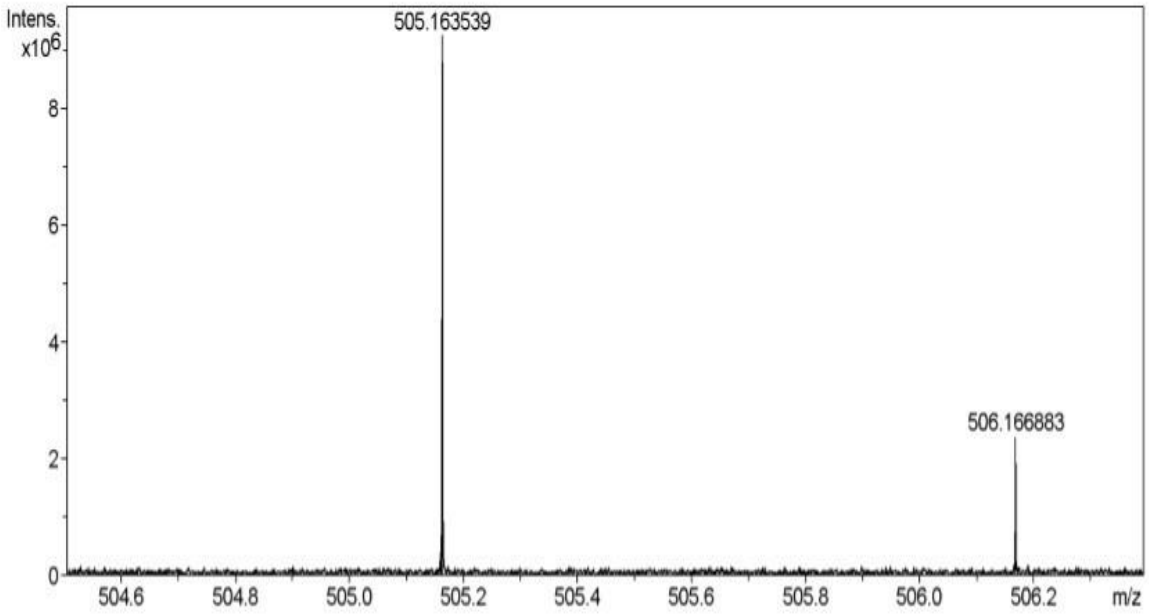

Figure A.3. High-resolution mass spectrum of L-PO_3H_2 in 1:1 THF:MeOH w/ NaCl. The expected molecular ions were observed with a difference of less than 1 ppm. Exact mass of $C_{26}H_{25}N_4O_5PNa^+$ = 505.163533 m/z Exact mass observed = 505.163539 m/z

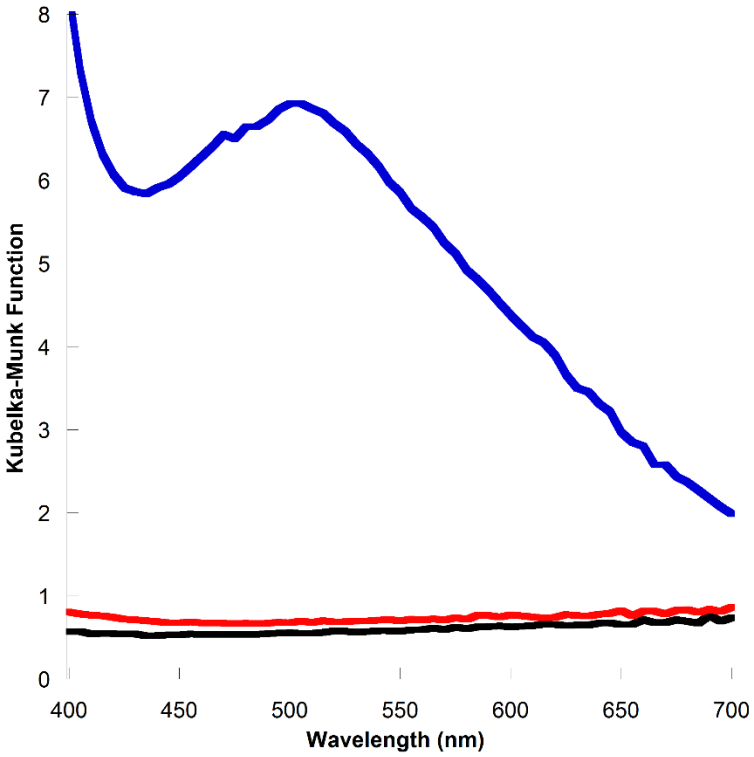

Figure A.4. Diffuse Reflectance UV-Vis spectra of thin film of bare ZrO_2 (black), L-PO_3H_2-ZrO_2 (red), and [$FeCl_2$(L-PO_3H_2)]-ZrO_2 (blue).

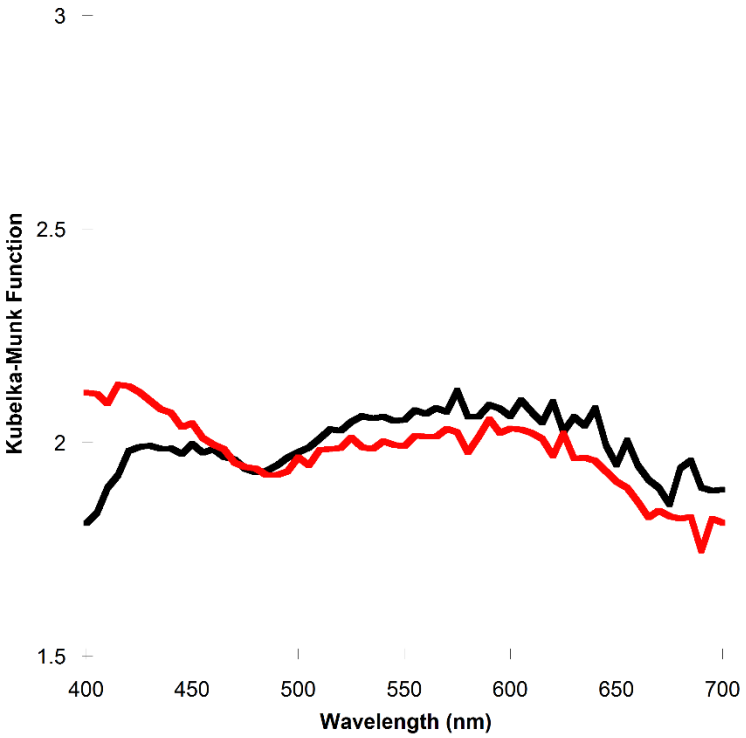

Figure A.5. Diffuse Reflectance UV-Vis spectra of thin film of bare $SrTiO_3$ (black) and $SrTiO_3$ thin film sensitized with $FeCl_3$ (red).

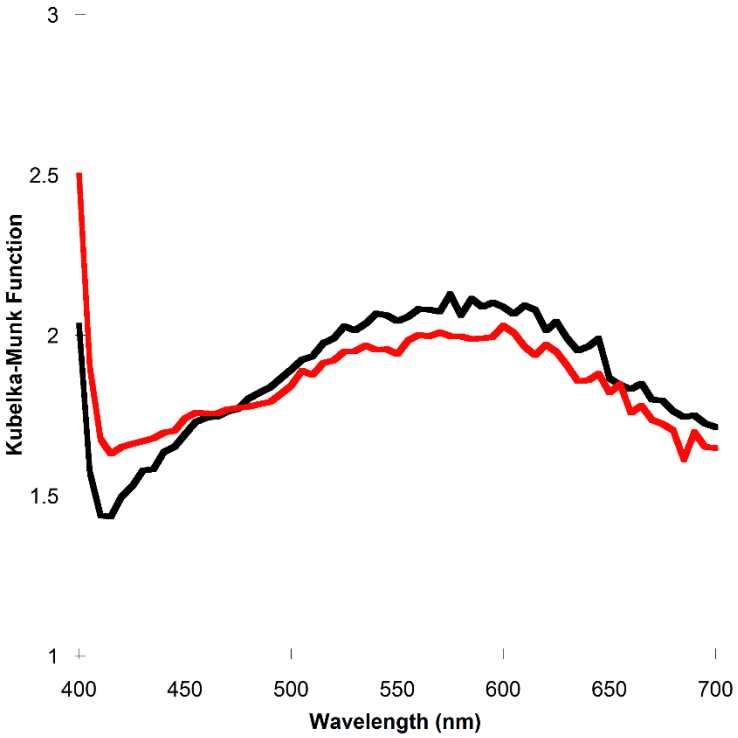

Figure A.6. Diffuse Reflectance UV-Vis spectra of thin film of bare TiO_2 (black) and TiO_2 thin film sensitized with $FeCl_3$ (red).

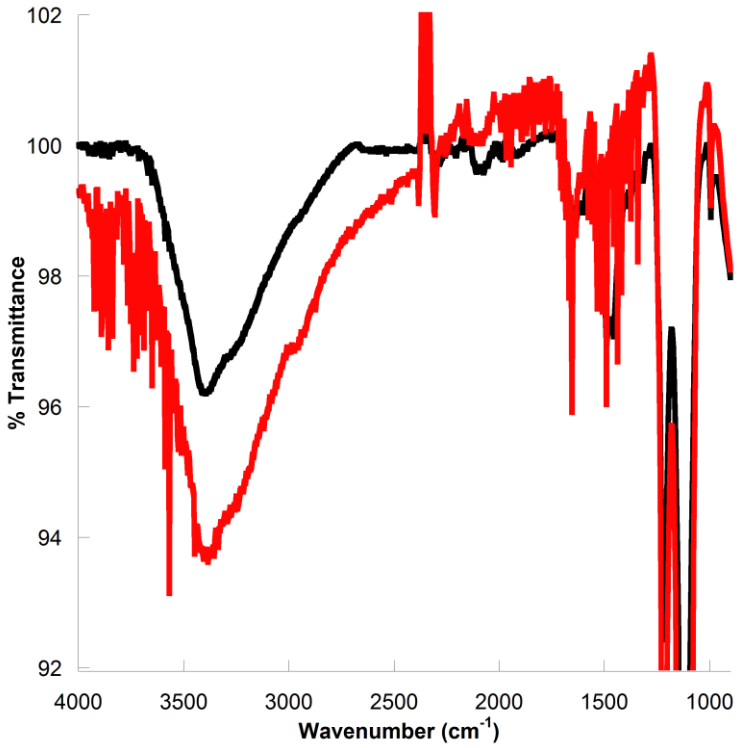

Figure A.7. Powder ATR-FTIR spectra of L-PO_3H_2-$SrTiO_3$ (black) and [$FeCl_2$(L-PO_3H_2)]-$SrTiO_3$ (red).

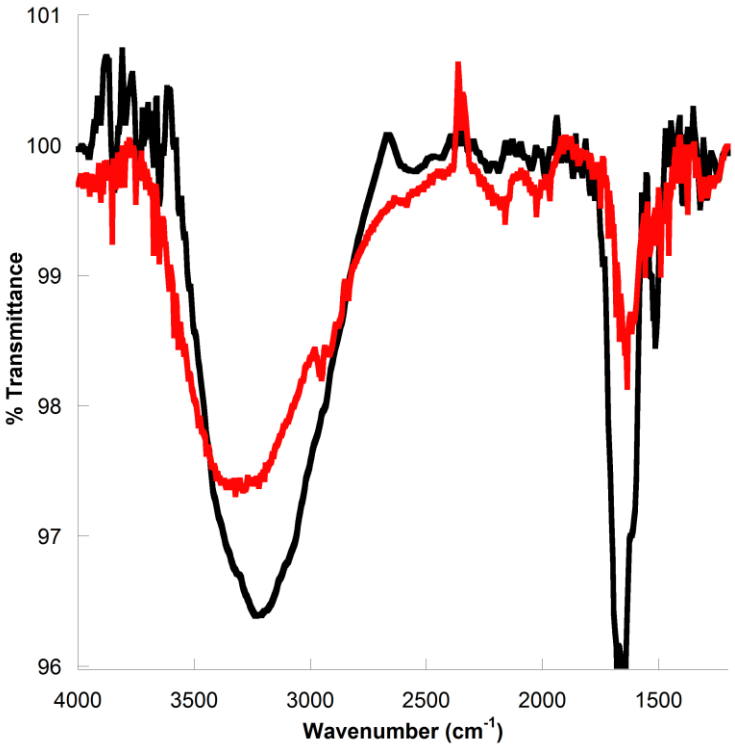

Figure A.8. Powder ATR-FTIR spectra of L-PO_3H_2-TiO_2 (black) and [$FeCl_2$(L-PO_3H_2)]-TiO_2 (red).

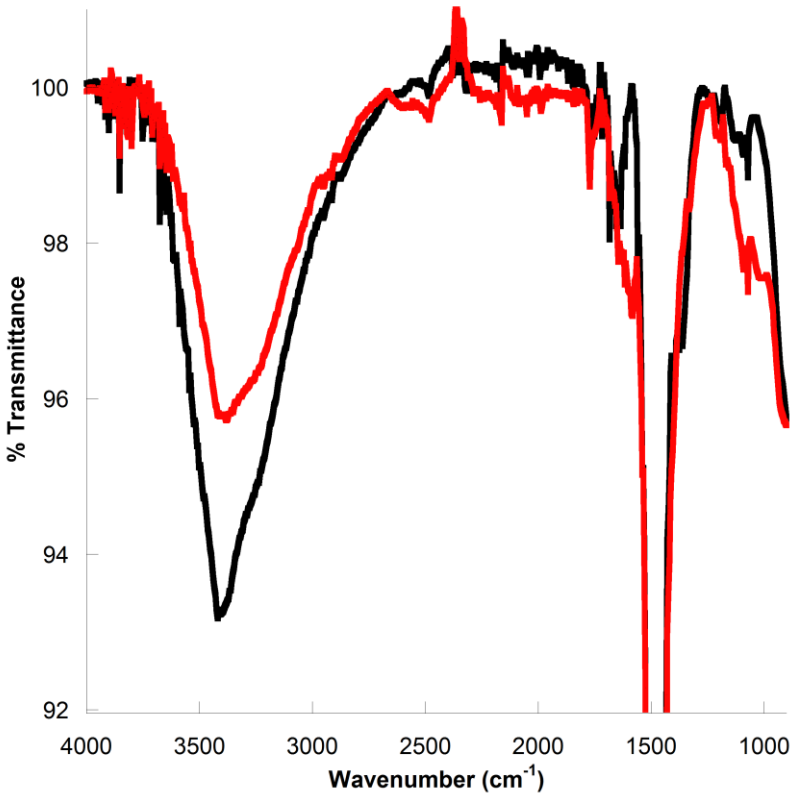

Figure A.9. Powder ATR-FTIR spectra of $SrTiO_3$ (black) and $SrTiO_3$ sensitized with fluorescein (red).

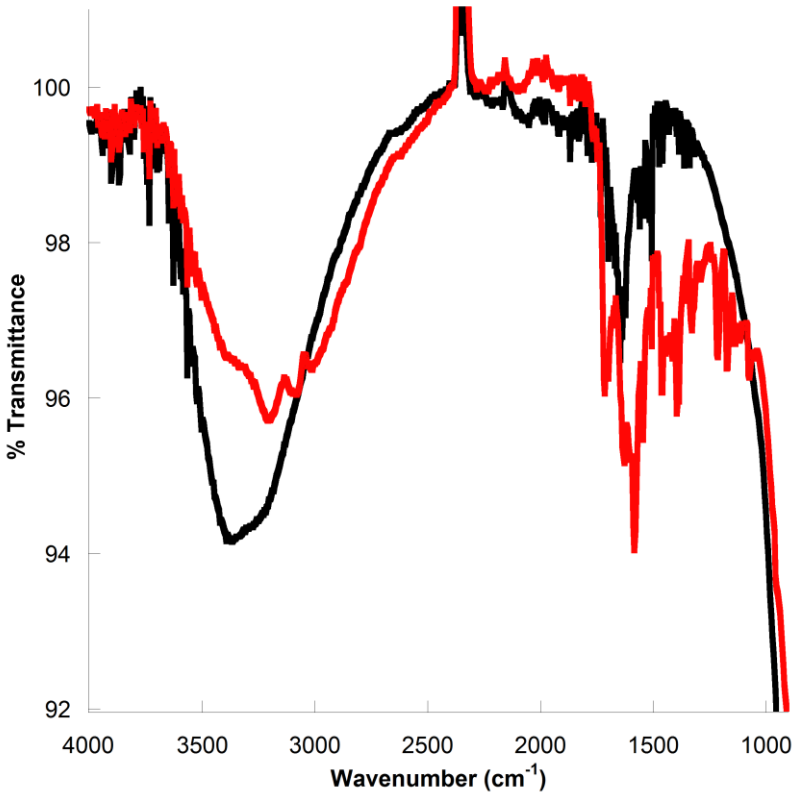

Figure A.10. Powder ATR-FTIR spectra of TiO_2 (black) and TiO_2 sensitized with fluorescein (red).

Chapter 3. Optimization of Photocatalytic Hydrogen Generation System

Introduction

Heterogeneous systems for photocatalytic hydrogen generation are of great interest as these systems overcome many of the limitations of homogeneous systems. One such limitation is diffusion, which is addressed in heterogeneous systems through the immobilization of the active catalyst on a solid support, such as a metal oxide semiconductor. Recovery of the catalyst within homogeneous systems is also very difficult, limiting the ability for the catalyst to be recycled. Immobilization of the catalyst on metal oxide semiconductors can lead to an increase in the stability of the catalyst and make it significantly easier to recycle the catalyst for continued use.

In one comparison of homogeneous and heterogeneous systems, Fan and coworkers found that immobilization of their molecular cobalt catalyst on TiO_2 nanoparticles led to a significant increase in hydrogen generation by the system.[1] This system, which incorporated the organic chromophore Eosin Y and triethylamine as the sacrificial donor, reached 90 TON after 6 hours of irradiation under optimal conditions.[1] Reisner and coworkers have also successfully immobilized a molecular cobalt complex on TiO_2 nanoparticles that is active for proton reduction.[2] Phosphonic acid groups were used to anchor both the cobaloxime complex and a ruthenium chromophore to the surface of the semiconductor. This system achieved only 53 TON after 8 hours of irradiation, in the presence of triethanolamine, due to the activity of the system decreasing after only two hours of irradiation.[2]

We have previously reported a family of iron polypyridyl catalysts that are active for homogeneous photocatalytic hydrogen evolution from aqueous solvent when paired with a chromophore and sacrificial electron donor.[3] Although these catalysts were found to be highly active compared to other homogeneous systems, reaching TON of 2100, it was of interest to determine if a related catalyst would show greater activity and stability in a heterogeneous system.[3] In the previous chapter it was shown that [$FeCl_2$(L-PO_3H_2)] was successfully immobilized on nanoparticles of multiple large band gap metal oxide semiconductors through a phosphonic acid anchoring group. Incorporating these nanoparticles into an AP system with a photosensitizer, such as fluorescein, and a sacrificial electron donor, such as triethylamine, would allow for photocatalytic hydrogen generation from aqueous solutions (Figure 3.1).

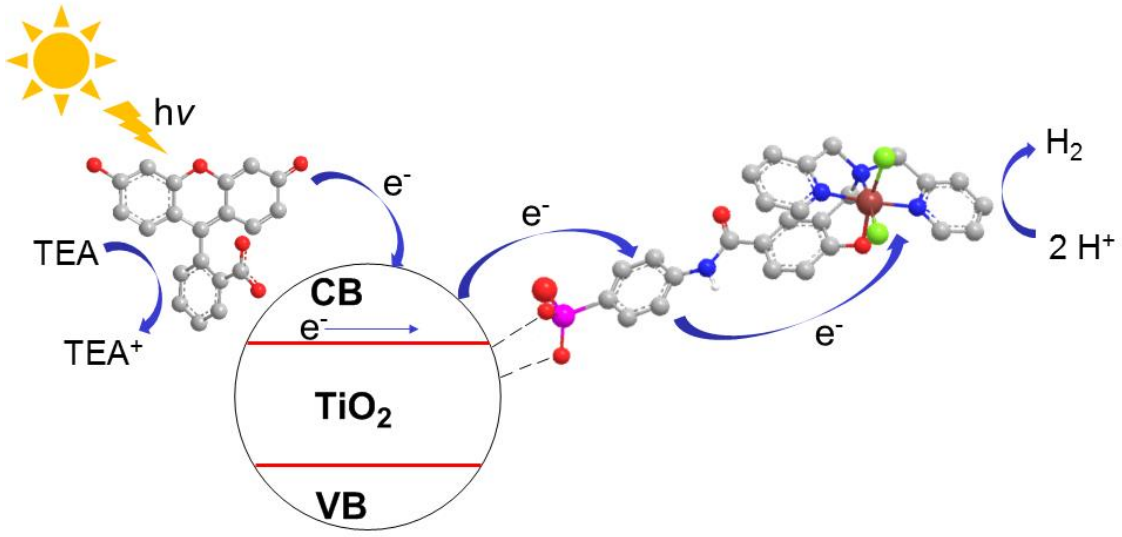

Figure 3.1. Scheme of proposed AP system for photocatalytic hydrogen generation from [$FeCl_2$(L-PO_3H_2)]-TiO_2 nanoparticles when paired with the photosensitizer fluorescein and sacrificial electron donor triethylamine.[4]

The work reported in this chapter illustrates the activity of the heterogeneous photocatalytic hydrogen generation system that incorporates [$FeCl_2$(L-PO_3H_2)]-sensitized semiconductor nanoparticles. Multiple aspects of the system were investigated to optimize the photocatalytic activity of the system. In addition, the durability of the [$FeCl_2$(L-PO_3H_2)]-sensitized nanoparticles was investigated to determine if the nanoparticles can be recycled over multiple experiments.

Experimental Procedure

Instrumentation

All UV-Vis analysis was performed using an Agilent Cary 60 Spectrophotometer. All GC analysis was performed using a Bruker Scion 436 gas chromatograph with argon carrier gas and a molecular sieve column.

Surface Coverage Determination

UV-Vis spectrophotometry was used to determine the coverage of ligand on the surface of the metal oxide semiconductor nanoparticles as outlined in previously reported procedures.[5] A 2.5 x 10^{-5} M solution of L-PO_3H_2 in methanol was prepared and analyzed via UV-Vis spectrophotometry. 4.0 mL of the L-PO_3H_2 solution was then added to a sample vial with 5.0 mg of semiconductor. The sample vial was capped and the mixture was stirred for one hour. After stirring, the mixture was divided into microcentrifuge tubes and centrifuged at 13,400 rpm for 15 minutes. After centrifugation, the supernatant was collected and analyzed via UV-Vis spectrophotometry. The absorbance of the supernatant was compared to the absorbance of the original L-PO_3H_2 solution at 295 nm. The difference in absorbance at 295 nm between the L-PO_3H_2 stock solution and collected supernatant was used to calculate the number of moles of L-PO_3H_2 immobilized on the surface of the semiconductor nanoparticles. A sample calculation is shown below:

$$mol\ \mathrm{LP}O_3H_2 = \left[1 - \left(\frac{supernatant\ abs.}{original\ ligand\ solution\ abs.}\right)\right] \times (2.5 \times 10^{-5} M) \times (4 \times 10^{-3} L)$$

$$mol\ \mathrm{LP}O_3H_2 = \left[1 - \left(\frac{0.047917}{0.324828}\right)\right] \times (2.5 \times 10^{-5} M) \times (4 \times 10^{-3} L)$$

$$mol\ \mathrm{LP}O_3H_2 = 8.52 \times 10^{-8}\ moles\ per\ 5\ mg\ nanoparticles$$

It was assumed that all of the ligand immobilized on the semiconductor surface would complex with $FeCl_3$ to form the catalyst. Because of this, it was assumed that the moles of [$FeCl_2$(L-PO_3H_2)] on the semiconductor surface was equivalent to the calculated number of moles of L-PO_3H_2 immobilized on the semiconductor surface for a given mass of nanoparticles.

GC Calibration

Two 500 mL round bottom flasks were evacuated and then filled with CH_4 and H_2 gas, one in each flask, and sealed with an airtight septum secured with copper wire. A sample was then prepared in a test tube containing a solution of 2.0 mL of CH_3CN and 2.0 mL of DI water. The sample was sealed with a rubber septum, secured with copper wire, and degassed under Ar for approximately 15 minutes. A 10.0 mL Hamilton gastight syringe was then used to remove 1.0 mL of headspace gas from the test tube and 1.0 mL of CH_4 was added as an internal standard. Varied amounts of H_2 gas, ranging from 10 µL to 500 µL, were then added to the test tube. Gas samples of 100 µL each were injected into a GC to

determine the ratio of peak areas of H_2 to CH_4. The peak area ratios were then plotted versus the volume of H_2. The slope of the linear trend of the data was used to calculate the volume of H_2 generated from hydrogen evolution studies (Figure 3.2).

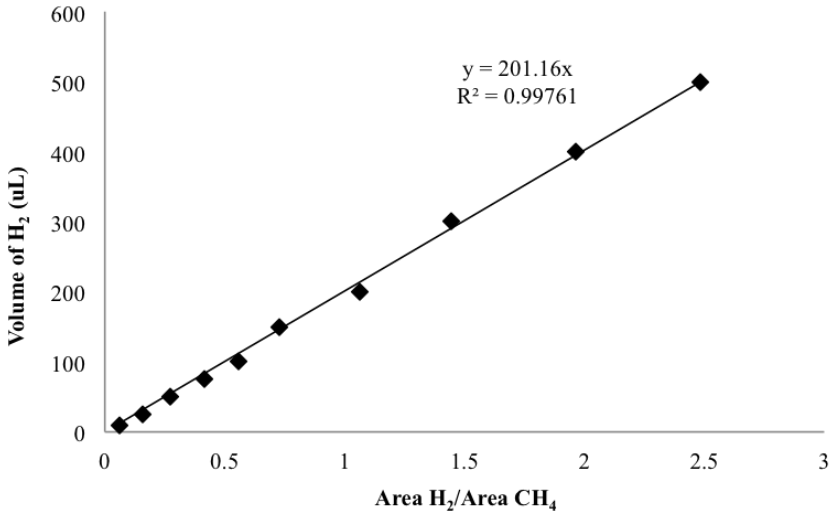

Figure 3.2. Calibration curve of H_2 to CH_4 peak areas used for determination of hydrogen generation. The ratio of peak areas was plotted against the volume of H_2 injected into the GC.

Calculation of Turnover Number (TON)

For the purposes of our photochemistry studies, turnover number (TON) may be defined as the number of moles of hydrogen generated per mole of catalyst present in the system. Utilizing the calibration curve shown previously, it is possible to determine the volume of hydrogen generated by our photochemical system within our reaction vessel from the ratio of the peak areas of H_2 and CH_4 from our GC analysis. Our calibration curve shows that the volume of hydrogen

generated by the system has a linear relationship to the peak area ratio of the H_2 to CH_4 with a slope of 201.16, as shown by the relationship[3]:

$$\mu L\ H_2 = 201.16\left(\frac{Area\ H_2}{Area\ CH_4}\right)$$

A sample calculation is included below:

$$\mu L\ H_2 = 201.16\left(\frac{525021}{35747.5}\right) = 2954$$

$$2954\ \mu L\ H_2 \times \frac{1\ L}{1 \times 10^6\ \mu L} \times \frac{1\ mol}{22.4\ L} = 1.32 \times 10^{-4}\ mol\ H_2$$

$$\frac{1.32 \times 10^{-4}\ mol\ H_2}{1.68 \times 10^{-8}\ mol\ catalyst} = 7850\ TON$$

Photochemistry Studies

Samples for hydrogen evolution studies were prepared as 1:1 ethanol:water mixtures in 16 x 125 mm glass test tubes through the addition of a measured mass of semiconductor nanoparticles, chromophore in ethanol, and 5% by volume sacrificial electron donor in deionized water, in the order listed. The total volume of the mixture in each test tube was 4.0 mL. Prior to the addition of sacrificial donor solution, the test tubes were covered with aluminum foil to prevent light exposure. Sacrificial donor solution was then added to the mixtures followed by capping test tubes with septa. The test tubes were then sealed with copper wire prior to degassing the mixtures for 10 minutes with argon. After degassing, a Hamilton gas syringe was used to remove 1.0 mL of headspace

from each test tube and add 1.0 mL methane as an internal standard. The aluminum foil covers were then removed and test tubes were placed in a rotating apparatus where the mixtures were irradiated with green light-emitting diodes (λ = 520 nm, 0.12 W) while stirring for a predetermined amount of time. After irradiation, a Hamilton gas syringe was used to remove 0.10 mL of headspace gas from each test tube and injected into a gas chromatograph for analysis.

Catalyst Stability Study

Samples were prepared in an identical manner as previously described photochemistry studies. Each sample contained 5 mg of $[FeCl_2(L\text{-}PO_3H_2)]$-sensitized nanoparticles, 2.0 mM fluorescein in ethanol, and 5% v/v triethylamine in deionized water. Degassing, irradiation, and headspace gas analysis were performed in an identical fashion to previous photochemistry studies. Following GC analysis of the headspace gas after 31 hours of irradiation, the samples were removed from the LED set-up and the mixtures were transferred to centrifuge tubes. The mixtures were then centrifuged for 12 minutes at 5,000 rpm. Following centrifugation, the chromophore and sacrificial donor mixture was removed from each sample. The remaining nanoparticles were rinsed with ethanol, followed by the addition of fresh fluorescein solution. The nanoparticles and fluorescein solution were then transferred back to the original 16 x 125 mm glass test tubes, capped with new rubber septa, and sealed with copper wire. The test tubes were then covered with aluminum foil to prevent light exposure, followed by addition of fresh triethylamine in deionized water solution to the mixtures using a syringe.

Mixtures were then degassed for 10 minutes with argon. Following degassing, a Hamilton gas syringe was used to remove 1.0 mL of headspace gas from each test tube and add 1.0 mL methane as an internal standard. The aluminum foil covers were then removed and the test tubes were returned to the LED set-up for irradiation while stirring. GC analysis of the headspace gas of the samples was then performed after 3, 6, and 12 hours of irradiation by removing 0.10 mL of headspace gas with a Hamilton gas syringe and injecting into the gas chromatograph.

Control Experiments

No semiconductor: Identical amount of L-PO_3H_2 and $FeCl_3$ as amount of catalyst calculated to be on 1 mg of [$FeCl_2$(L-PO_3H_2)]-sensitized semiconductor nanoparticles added directly to mixtures. Photochemistry studies then performed with optimal chromophore and sacrificial donor conditions for hydrogen generation.

No chromophore: [$FeCl_2$(L-PO_3H_2)]-sensitized semiconductor nanoparticles were prepared via the centrifuge method previously described. 2.0 mL of ethanol was added to each mixture rather than chromophore in ethanol solution to maintain 1:1 ethanol:water ratio of mixture. All other conditions and procedures performed in identical manner to typical photochemistry experiments.

No L-PO_3H_2: Semiconductor thin films prepared via the doctor blading technique previously described were placed in a petri dish wrapped in aluminum foil.

Excess $FeCl_3$ (8.0×10^{-7} moles) in methanol was added to the petri dish with excess methanol to ensure the thin film was completely submerged. The petri dish was then covered with a watch glass and aluminum foil to prevent light exposure. After soaking for 30 minutes in $FeCl_3$ solution, the thin film was removed from the petri dish and rinsed with methanol. The thin films were allowed to dry in the dark overnight. These nanoparticles were then used for photochemistry studies under optimal conditions for hydrogen generation.

No Fe: L-PO_3H_2 was immobilized on semiconductor nanoparticles via the centrifuge method previously described. After final centrifugation of L-PO_3H_2-sensitized nanoparticles in methanol, the supernatant was removed and the Eppendorf tubes containing the nanoparticles were left open in the dark to dry overnight. These nanoparticles were then used to perform photochemistry studies under optimal conditions for hydrogen generation.

Results and Discussion

Photocatalytic hydrogen evolution

In order to begin to optimize our photocatalytic system with [$FeCl_2$(L-PO_3H_2)]-functionalized nanoparticles, it was necessary to determine the components best suited for the photochemical system. The first component that was investigated was the sacrificial electron donor, which provides the electrons required to reduce the chromophore or catalyst.[6] We chose to study triethylamine (TEA) and triethanolamine (TEOA) as these are two common sacrificial electron donors for photocatalytic proton hydrogen generation systems.[1,2,3,6] To determine which sacrificial donor was better suited for our system, we conducted a study in which 5% sacrificial donor solution in deionized water was paired with 1.9 mM fluorescein in ethanol, to act as the photosensitizer, and 5 mg [$FeCl_2$(L-PO_3H_2)]-$SrTiO_3$ nanoparticles. After 18 hours of irradiation, mixtures containing TEA as the sacrificial donor species generated 1900 µL of hydrogen gas, corresponding to a TON of 1000. Mixtures containing TEOA generated only 250 µL of hydrogen gas, equivalent to a TON of 130 (Table 3.1).

Table 3.1. Hydrogen generation of mixtures of 5 mg [$FeCl_2$(L-PO_3H_2)]-$SrTiO_3$ nanoparticles, 1.9 mM fluorescein, and 5% v/v sacrificial donor in 1:1 ethanol:water after 18 hours of irradiation.

Sacrificial Donor	H_2 Generated (µL)	TON
Triethylamine	1900	1000
Triethanolamine	250	130

Although TEA is often paired with fluorescein in photochemical systems, we also investigated the activity of our system when the chromophore Eosin Y was used as the photosensitizer.[3,7,8] A photochemistry study was performed in which 1.9 mM of chromophore in ethanol was combined with 5% v/v triethylamine and 1 mg $[FeCl_2(L\text{-}PO_3H_2)]$-$SrTiO_3$ nanoparticles in 1:1 ethanol:water mixtures and irradiated for 24 hours. Mixtures containing Eosin Y generated only 280 µL of hydrogen, equivalent to 750 TON (Table 3.2). The difference in activity of mixtures containing fluorescein and Eosin Y may be attributable to fluorescein having a more reducing excited state than Eosin Y.[6] This makes electron transfer to $[FeCl_2(L\text{-}PO_3H_2)]$-$SrTiO_3$ nanoparticles from the excited state of fluorescein more favorable. This indicated that pairing fluorescein and triethylamine, as the photosensitizer and sacrificial donor species, respectively, was the most efficient combination for hydrogen evolution.

Table 3.2. Hydrogen generation of mixtures of 1 mg $[FeCl_2(L\text{-}PO_3H_2)]$-$SrTiO_3$ nanoparticles, 2.0 mM chromophore, and 5% v/v triethylamine in 1:1 ethanol:water after 24 hours of irradiation.

Chromophore	H_2 Generated (µL)	TON
Fluorescein	1800	4700
Eosin Y	280	750

It was also of interest to determine if the preparation method of the $[FeCl_2(L\text{-}PO_3H_2)]$-sensitized nanoparticles impacted the activity of the photochemical system. To accomplish this, we conducted a study in which the activity of $[FeCl_2(L\text{-}PO_3H_2)]$-$SrTiO_3$ nanoparticles prepared via the thin film

method was compared to the activity of [$FeCl_2$(L-PO_3H_2)]-$SrTiO_3$ nanoparticles prepared via the centrifuge method. For this study, 1.9 mM fluorescein and 5% v/v TEA were added to 5 mg [$FeCl_2$(L-PO_3H_2)]-$SrTiO_3$ nanoparticles prepared via the thin film or centrifuge method in 1:1 ethanol:water mixtures and irradiated for 18 hours. Mixtures containing [$FeCl_2$(L-PO_3H_2)]-$SrTiO_3$ prepared via the thin film method generated 1900 µL of hydrogen gas, corresponding to a TON of 1000. The [$FeCl_2$(L-PO_3H_2)]-$SrTiO_3$ nanoparticles prepared via the centrifuge method were found to be slightly more active, achieving a TON of 1100, corresponding to the evolution of 2100 µL of hydrogen gas (Table 3.3). This increase in activity is most likely due to the fact that only one side of the semiconductor thin films is accessible for binding L-PO_3H_2. The centrifuge prepared semiconductor nanoparticles do not face this surface area limitation during the sensitization procedure.

Table 3.3. Hydrogen generation of mixtures of 5 mg [$FeCl_2$(L-PO_3H_2)]-$SrTiO_3$ nanoparticles, 1.9 mM fluorescein, and 5% v/v triethylamine in 1:1 ethanol:water after 18 hours of irradiation.

Nanoparticle Preparation Method	H_2 Generated (µL)	TON
Thin Film	1900	1000
Centrifuge	2100	1100

The next aspect of our system that was examined was the mass of [$FeCl_2$(L-PO_3H_2)]-sensitized semiconductor nanoparticles added to the reaction mixtures. A study was designed in which mixtures of varied mass of [$FeCl_2$(L-PO_3H_2)]-$SrTiO_3$ nanoparticles, 1.9 mM fluorescein, and 5% v/v triethylamine were

prepared in a final ratio of 1:1 ethanol:water. Samples were then irradiated for 24 hours prior to analysis of the headspace gas to determine activity (Table 3.4).

Table 3.4. Hydrogen generation of mixtures of $[FeCl_2(L\text{-}PO_3H_2)]$-$SrTiO_3$ nanoparticles, 1.9 mM fluorescein, and 5% v/v triethylamine in 1:1 ethanol:water after 24 hours irradiation.

Nanoparticle Description	1 mg		2.5 mg		5 mg	
	H_2 Generated (µL)	TON	H_2 Generated (µL)	TON	H_2 Generated (µL)	TON
$[FeCl_2(L\text{-}PO_3H_2)]$-$SrTiO_3$	1200	3100	1600	1600	2000	1100

Although it was observed that significant volumes of hydrogen gas were generated in all samples, the TON of each sample was of greater use for comparing activity in this particular study. This was due to the vast differences in the amount of catalyst added to each sample through the addition of different masses of nanoparticles. Although samples containing 5 mg $[FeCl_2(L\text{-}PO_3H_2)]$-$SrTiO_3$ generated approximately 2000 µL of H_2, these samples achieved only 1100 TON. The relative activity of samples containing 1 mg FeP-$SrTiO_3$ was significantly greater than samples containing 5 mg of nanoparticles, surpassing 3100 TON. The relatively small increase in the volume of H_2 generated in samples containing 5 mg $[FeCl_2(L\text{-}PO_3H_2)]$-$SrTiO_3$ may be attributed to faster degradation of the sacrificial electron donor or chromophore. It is also possible that the concentration of aqueous protons within the reaction mixture acts as a limiting reagent within the system, therefore slowing the rate of hydrogen generation. Studies were also performed in which less than 1 mg of $[FeCl_2(L\text{-}$

PO_3H_2)]-$SrTiO_3$ was added to samples, however it proved difficult to reliably obtain this mass of nanoparticles and the photochemical system appeared to degrade much more quickly than in previous studies.

Mass optimization studies were also performed with $FeCl_2$(L-PO_3H_2)]-TiO_2 nanoparticles. In this study, mixtures of a varied mass of [$FeCl_2$(L-PO_3H_2)]-TiO_2 nanoparticles, 1.9 mM fluorescein, and 5% v/v triethylamine in 1:1 ethanol:water were prepared and irradiated for 24 hours. After 24 hours, the headspace gas of the samples was analyzed to measure hydrogen generation (Table 3.5).

Table 3.5. Hydrogen generation of mixtures of [$FeCl_2$(L-PO_3H_2)]-TiO_2 nanoparticles, 1.9 mM fluorescein, and 5% v/v triethylamine in 1:1 ethanol:water after 24 hours irradiation.

Nanoparticle Description	**1 mg**		**5 mg**	
	H_2 Generated (µL)	**TON**	**H_2 Generated (µL)**	**TON**
[$FeCl_2$(L-PO_3H_2)]-TiO_2	2000	5300	2700	1400

The trend observed relating the mass of [$FeCl_2$(L-PO_3H_2)]-$SrTiO_3$ nanoparticles to TON was also observed with [$FeCl_2$(L-PO_3H_2)]-TiO_2 nanoparticles. Although a greater volume of hydrogen was generated from mixtures containing 5 mg of [$FeCl_2$(L-PO_3H_2)]-TiO_2, mixtures containing 1 mg of [$FeCl_2$(L-PO_3H_2)]-TiO_2 showed greater activity, generating 5300 TON. Once again, samples containing 5 mg of nanoparticles generated a greater volume of H_2, 2700 µL compared to 2000 µL for mixtures containing 1 mg of nanoparticles.

However, this difference in H_2 generation is relatively small considering the significant difference in the amount of catalyst added to each mixture.

After determining the optimal mass of [$FeCl_2$(L-PO_3H_2)]-$SrTiO_3$ nanoparticles for photocatalytic hydrogen generation, the optimal concentration of chromophore was investigated. In these studies, 1 mg [$FeCl_2$(L-PO_3H_2)]-$SrTiO_3$ nanoparticles were added to a varied concentration of fluorescein and 5% v/v triethylamine in 1:1 ethanol:water mixtures. Analysis of the headspace gas of the mixtures was performed after 24 hours of irradiation. These studies showed a clear relationship between the concentration of fluorescein and the photocatalytic activity of our system (Figure 3.3).

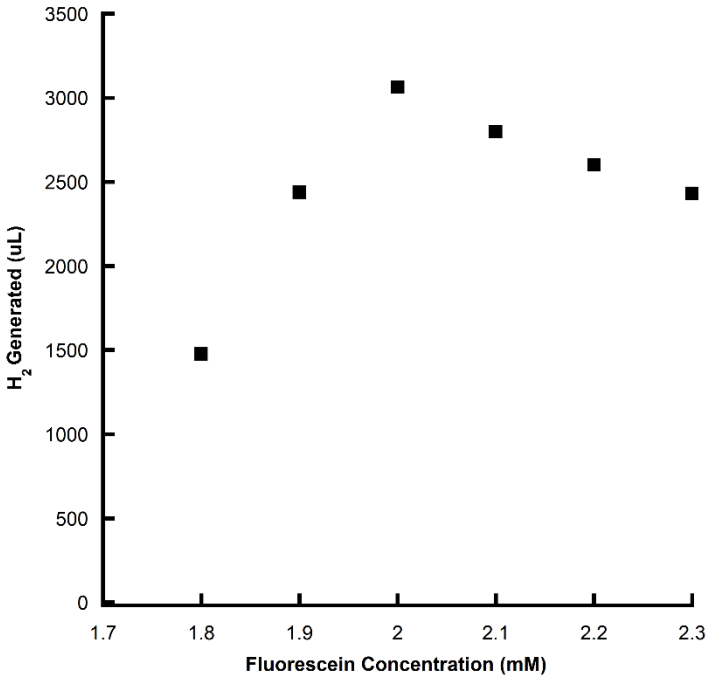

Figure 3.3. Hydrogen generation from mixtures containing 1 mg [$FeCl_2$(L-PO_3H_2)]-$SrTiO_3$ as a function of fluorescein concentration. Results after 24 hours of irradiation when paired with 5% v/v triethylamine.

The optimal concentration of fluorescein for photocatalytic hydrogen generation was determined to be 2.0 mM. The decrease in hydrogen generation observed at fluorescein concentrations less than 2.0 mM may be attributable to less aggregation of the chromophore on the semiconductor nanoparticle surface, thus decreasing the amount of visible light absorbed by the system. At fluorescein concentrations greater than 2.0 mM there may be issues with solubility of the chromophore in the 1:1 ethanol:water reaction mixtures. In addition, self-quenching of fluorescein may occur at increased photosensitizer concentration, thus causing the observed decrease in activity of the system.[7,8]

After establishing the proton reduction activity of the [$FeCl_2$(L-PO_3H_2)]-sensitized nanoparticles within our photochemical system, control experiments were performed to ensure that all components of the system were necessary for photocatalytic hydrogen generation (Table 3.6). Ensuring that the observed hydrogen generation was catalyzed by the immobilized molecular iron catalyst was of particular interest, as the photocatalytic activity of semiconductor materials has been shown to be enhanced through transition metal doping.[9,10]

Table 3.6. Hydrogen generation of mixtures of 1 mg nanoparticles, 2.0 mM fluorescein, and 5% v/v triethylamine in 1:1 ethanol:water after 24 hours of irradiation.

Nanoparticle Description	H_2 Generated (μL)
$SrTiO_3$	81
L-PO_3H_2-$SrTiO_3$	360
Fe-$SrTiO_3$	90
[$FeCl_2$(L-PO_3H_2)]-$SrTiO_3$	1900
TiO_2	37
L-PO_3H_2-TiO_2	150
Fe-TiO_2	230
[$FeCl_2$(L-PO_3H_2)]-TiO_2	2300

The control studies demonstrated that all components of the photochemical system were necessary for significant hydrogen generation. Activity of the system was evaluated by comparing the volume of H_2 generated in control studies to the volume of H_2 generated under optimal conditions, as catalyst was not present in all control studies. The control studies with the highest activity generated approximately an order of magnitude less H_2 than the [$FeCl_2$(L-PO_3H_2)]-sensitized semiconductor nanoparticles in our optimal conditions. Control studies performed with bare $SrTiO_3$ and TiO_2 nanoparticles generated less than 100 μL of H_2, further indicating that the immobilized molecular catalyst drives proton reduction within the photochemical system. Additional control studies that excluded either metal oxide semiconductor or chromophore showed no hydrogen generation by the photochemical system. These results indicate that all aspects of the photochemical system are necessary for significant hydrogen generation. The results of these control

experiments also demonstrate that hydrogen generation is being catalyzed by the [$FeCl_2$(L-PO_3H_2)]-sensitized nanoparticles.

Another aspect of our photochemical system that we sought to optimize was the pH of the reaction mixture. To investigate the effect of pH on the photocatalytic activity of the system, we conducted photochemistry studies in which the pH of the sacrificial donor solution was varied. The pH of the sacrificial donor solution in all previous photochemistry studies was measured to be 12.5 (triethylamine pKa = 10.75). Combining 5% v/v triethylamine solution at this pH with 2.0 mM fluorescein in ethanol and 1 mg of nanoparticles resulted in 5100 TON and 6100 TON for samples containing [$FeCl_2$(L-PO_3H_2)]-$SrTiO_3$ and [$FeCl_2$(L-PO_3H_2)]-TiO_2, respectively, after 24 hours of irradiation. When the pH of the sacrificial donor solution was lowered using 1 M HCl, a significant decrease in the photocatalytic activity of the system for mixtures containing [$FeCl_2$(L-PO_3H_2)]-$SrTiO_3$ or [$FeCl_2$(L-PO_3H_2)]-TiO_2 was observed (Table 3.7). A trend was observed indicating that lowering the pH of the sacrificial donor solution caused a decrease in the photocatalytic activity of the system. At pH 9 mixtures containing [$FeCl_2$(L-PO_3H_2)]-$SrTiO_3$ generated a negligible volume of hydrogen while mixtures containing [$FeCl_2$(L-PO_3H_2)]-TiO_2 generated no hydrogen at all, corresponding to 4 and 0 TON respectively. It is possible that the observed trend is caused by degradation of fluorescein as previous studies have shown that fluorescein decomposes much more rapidly at pH below 12.[8] It has also been found that it is more difficult to oxidize TEA at low pH, making it a less effective electron donor within the photochemical system.[11]

Interestingly, it was also observed that the photocatalytic activity of the system decreased as the pH of the sacrificial donor solution was adjusted to pH greater than 12.5. At pH 13.5, mixtures containing [$FeCl_2$(L-PO_3H_2)]-$SrTiO_3$ generated only 310 µL of hydrogen gas while mixtures containing [$FeCl_2$(L-PO_3H_2)]-TiO_2 generated only 130 µL of hydrogen gas, corresponding to 800 and 350 TON respectively. This decrease in activity can most likely be attributed to a decrease in the amount of hydrogen ions present in solution at extremely basic pH. These studies indicated that the optimal pH of the sacrificial donor solution for photocatalytic hydrogen generation was 12.5.

Table 3.7. Hydrogen generation of mixtures of 1 mg [$FeCl_2$(L-PO_3H_2)]-sensitized nanoparticles, 2.0 mM fluorescein, and 5% v/v triethylamine in 1:1 ethanol:water adjusted to listed pH after 24 hours of irradiation.

Nanoparticle Description	pH of Sacrificial Donor Solution	H_2 Generated (µL)	TON
[$FeCl_2$(L-PO_3H_2)]-$SrTiO_3$	9	1.4	4
[$FeCl_2$(L-PO_3H_2)]-$SrTiO_3$	10	200	500
[$FeCl_2$(L-PO_3H_2)]-$SrTiO_3$	11	550	1400
[$FeCl_2$(L-PO_3H_2)]-$SrTiO_3$	12.5	1900	5100
[$FeCl_2$(L-PO_3H_2)]-$SrTiO_3$	13	950	2500
[$FeCl_2$(L-PO_3H_2)]-$SrTiO_3$	13.5	310	800
[$FeCl_2$(L-PO_3H_2)]-TiO_2	9	0	0
[$FeCl_2$(L-PO_3H_2)]-TiO_2	10	190	500
[$FeCl_2$(L-PO_3H_2)]-TiO_2	11	1400	3500
[$FeCl_2$(L-PO_3H_2)]-TiO_2	12.5	2300	6100
[$FeCl_2$(L-PO_3H_2)]-TiO_2	13	220	600
[$FeCl_2$(L-PO_3H_2)]-TiO_2	13.5	130	350

After determining the optimal conditions for H_2 generation within our system, it was of interest to investigate the photocatalytic activity of the system over time. To accomplish this, a study was conducted in which mixtures were prepared under the previously described optimal conditions with either 1 mg $[FeCl_2(L\text{-}PO_3H_2)]$-$SrTiO_3$ or 1 mg $[FeCl_2(L\text{-}PO_3H_2)]$-$TiO_2$. GC analysis of the headspace gas of samples were taken after 1, 3, 6, 12, 18, 24, 28, and 31 hours of irradiation (Figure 3.4).

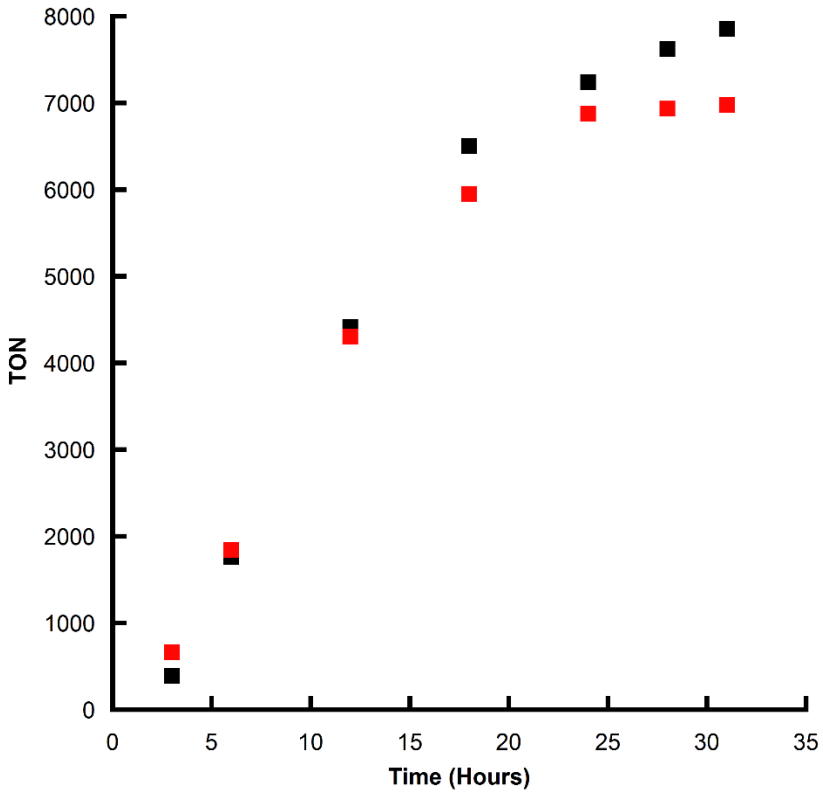

Figure 3.4. Hydrogen generation expressed as TON from mixtures containing 1 mg $[FeCl_2(L\text{-}PO_3H_2)]$-$SrTiO_3$ (red) and $[FeCl_2(L\text{-}PO_3H_2)]$-$TiO_2$ (black) with 2 mM fluorescein and 5% v/v triethylamine in 1:1 ethanol:water.

After 31 hours of irradiation, $[FeCl_2(L\text{-}PO_3H_2)]$-$TiO_2$ nanoparticles were found to be more active than $[FeCl_2(L\text{-}PO_3H_2)]$-$SrTiO_3$, nanoparticles, with mixtures generating 7800 TON and 7000 TON respectively. Interestingly, it was observed that H_2 was initially generated at a faster rate by mixtures containing $[FeCl_2(L\text{-}PO_3H_2)]$-$SrTiO_3$. However, after approximately 6 hours of irradiation the rate of hydrogen generation from mixtures containing $[FeCl_2(L\text{-}PO_3H_2)]$-$SrTiO_3$ began to decrease while mixtures containing $[FeCl_2(L\text{-}PO_3H_2)]$-$TiO_2$ nanoparticles maintained a near-constant rate of hydrogen generation until approximately 24 hours of irradiation. This suggests that decomposition of the system occurs more rapidly in mixtures containing $[FeCl_2(L\text{-}PO_3H_2)]$-$SrTiO_3$.

As stated previously, one of the goals of immobilizing the Fe catalyst on metal oxide semiconductors is to increase the durability and stability of the photocatalytic system. One benefit of increased stability would be the ability to recycle $[FeCl_2(L\text{-}PO_3H_2)]$-sensitized nanoparticles for continued use in aqueous solution. The ability to recycle $[FeCl_2(L\text{-}PO_3H_2)]$-sensitized nanoparticles would also greatly reduce the cost of the prospective AP system. Based on the results of our study measuring photocatalytic activity of the $[FeCl_2(L\text{-}PO_3H_2)]$-sensitized nanoparticles over time, it was not immediately apparent if the decrease in the rate of hydrogen generation after 12-18 hours of irradiation was the result of decomposition of the catalyst, chromophore, or sacrificial electron donor. To investigate this further and determine if the $[FeCl_2(L\text{-}PO_3H_2)]$-sensitized semiconductor nanoparticles were recyclable, a hydrogen generation study was performed in which the chromophore and sacrificial donor solutions were

decanted following the cessation of hydrogen generation of our samples, followed by the addition of fresh chromophore and sacrificial donor solutions to the [$FeCl_2$(L-PO_3H_2)]-sensitized nanoparticles. The mixtures were then degassed again with argon and irradiated with GC samples taken at 3, 6, and 12 hours after the addition of fresh chromophore and sacrificial donor solutions. For this study, 5 mg of catalyst-sensitized nanoparticles were used to diminish the effect of lost nanoparticles during the decanting process and to increase the stability of our photochemical system. Because of this, the activity of our system has been expressed as total volume of hydrogen generated in Figure 3.5.

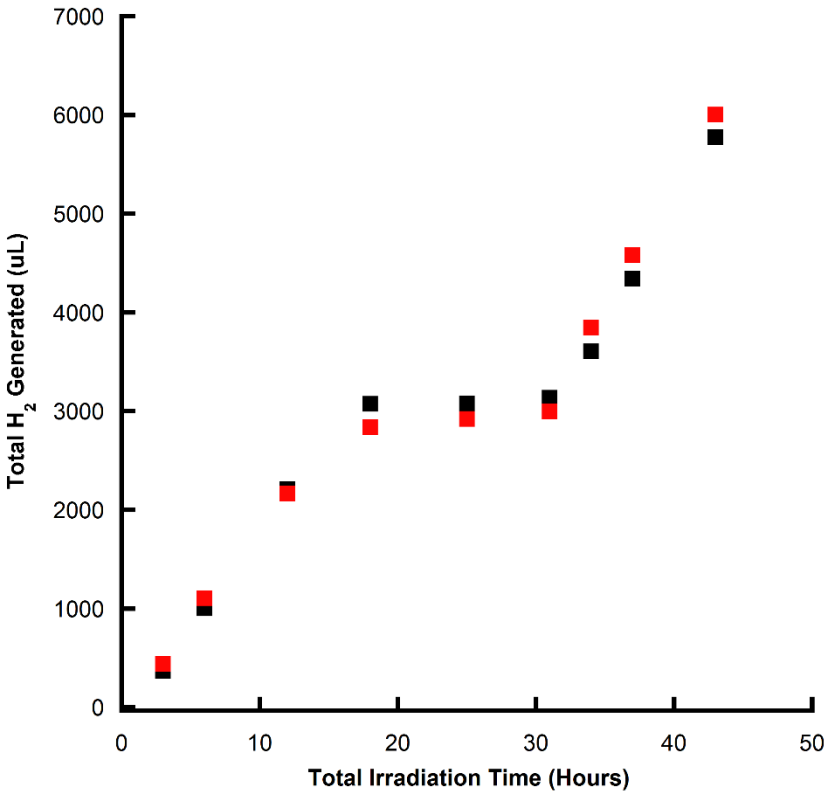

Figure 3.5. Hydrogen generation from mixtures containing 5 mg [$FeCl_2$(L-PO_3H_2)]-$SrTiO_3$ (red) and [$FeCl_2$(L-PO_3H_2)]-TiO_2 (black) with 2 mM fluorescein and 5% v/v triethylamine in 1:1 ethanol:water. After 31 hours of irradiation, the nanoparticles were collected and rinsed with ethanol and the solution was discarded. Fresh fluorescein and triethylamine solution was added to the nanoparticles and irradiation was resumed.

In the first 18 hours of irradiation prior to decanting the mixtures, the activity of the catalyst-sensitized nanoparticles followed the trend observed in previous studies. From 18-32 hours of irradiation hydrogen generation essentially ceased for mixtures containing both [$FeCl_2$(L-PO_3H_2)]-$SrTiO_3$ and [$FeCl_2$(L-PO_3H_2)]-TiO_2, suggesting degradation of our photochemical system. It was at this point that the mixtures were centrifuged and decanted, and the nanoparticles were rinsed with ethanol. Upon adding fresh chromophore and sacrificial donor solutions to the rinsed nanoparticles and returning the mixtures to the irradiation

set-up, we observed that hydrogen generation for both [$FeCl_2$(L-PO_3H_2)]-$SrTiO_3$ and [$FeCl_2$(L-PO_3H_2)]-TiO_2 mixtures returned to the previously observed rate. This suggests that the cessation of hydrogen generation observed after approximately 18 hours of irradiation was the result of chromophore or sacrificial donor degradation rather than decomposition of the [$FeCl_2$(L-PO_3H_2)]-sensitized semiconductor nanoparticles.

Conclusion

The work reported in this chapter outlines the development and optimization of a highly active and stable heterogeneous AP system for hydrogen generation. Under optimal conditions, mixtures containing [$FeCl_2$(L-PO_3H_2)]-$SrTiO_3$ surpass 7000 TON while mixtures containing [$FeCl_2$(L-PO_3H_2)]-TiO_2 surpass 7800 TON after 31 hours of irradiation. Both of these systems are significantly more active than previously reported heterogeneous systems for photocatalytic hydrogen generation (<100 TON). These systems are also significantly more active than the homogeneous system with the iron polypyridyl catalysts previously reported by our group (2100) TON. In addition, the [$FeCl_2$(L-PO_3H_2)]-sensitized semiconductor nanoparticles show extremely high stability as they can be recycled and added to fresh chromophore and sacrificial donor solutions. The recycled nanoparticles resume hydrogen generation at the same rate as initially observed, indicating no decomposition of the catalyst. This system holds great promise for larger-scale AP as it incorporates an iron-based proton reduction catalyst, inexpensive metal oxide semiconductor materials, and organic

chromophores. This noble-metal-free system with high activity may provide a path towards the development of cost-effective AP systems for water splitting.

References

1. Yin, M.; Ma, S.; Wu, C.; Fan, Y. A noble-metal-free photocatalytic hydrogen production system based on cobalt (III) complex and eosin Y-sensitized TiO_2. *RSC Adv.* **2015**, *5*, 1852-1858.
2. E. Reisner and F. Lakadamyali. Photocatalytic H_2 evolution from neutral water with a molecular cobalt catalyst on a dye-sensitised TiO_2 nanoparticle. *Chem. Commun.* **2011**, *47*, 1695-1697.
3. Hartley, C. L.; DiRisio, R. J.; Screen, M. E.; Mayer, K. J.; McNamara, W. R. Iron polypyridyl complexes for photocatalytic hydrogen generation. *Inorg. Chem.* **2016**, *55*, 8865-8870.
4. Race, N. A.; Zhang, W.; Screen, M. E.; Barden, B. A.; McNamara, W. R. Iron polypyridyl catalysts assembled on metal oxide semiconductors for photocatalytic hydrogen generation. *Chem Commun.*, **2018**, *54*, 3290-3293.
5. Lakadamyali, F.; Reynal, A.; Kato, M.; Durrant, J. R.; Reisner, E., Electron Transfer in Dye-Sensitized Semiconductors Modified with Molecular Cobalt Catalysts: Photoreduction of Aqueous Protons. *Chem. Eur. J.* **2012**, *18* (48), 15464-15475, S15464/1-S15464/18.
6. W. T. Eckenhoff and R. Eisenberg. Molecular systems for light driven hydrogen production. *Dalton Trans.* **2012**, *41*, 13004-13021.
7. Wise, C. F.; Liu, D.; Mayer, K. J.; Crossland, P. M.; Hartley, C. L.; McNamara, W. R. A nickel complex of a conjugated bis-dithiocarbazate Schiff base for the photocatalytic production of hydrogen. *Dalton Trans*. **2015**, *44*, 14265-14271.
8. Han, Z.; McNamara, W. R.; Eum, M-S.; Holland, P. L.; Eisenberg, R. A nickel thiolate catalyst for the long-lived photocatalytic production of hydrogen in a noble-metal free system. *Ang. Chem. Int. Ed.* **2012**, *51* (7), 1667-1670.
9. Hameed, A.; Gondal, M. A.; Yamani, Z. H. Effect of transition metal doping on photocatalytic activity of WO_3 for water splitting under laser illumination: role of 3d-orbitals. *Cat. Commun.* **2004**, *5* (11), 715-719.
10. Dholam, R.; Patel, N.; Adami, M.; Miotello, A. Hydrogen production by photocatalytic water-splitting using Cr- or Fe-doped TiO_2 composite thin films photocatalyst. *Int. J. Hydro. Energ.* **2009**, *34* (13), 5337-5346.
11. Zhang, P.; Wang, M.; Dong, J.; Li, X.; Wang, F.; Wu, L.; Sun, L. Photocatalytic hydrogen production from water by noble-metal-free molecular catalyst systems containing rose Bengal and the cobaloximes of BF_x-bridged oxime ligands. *J. Phys. Chem. C*, **2010**, *114* (37), 15878-15874.

Appendix B

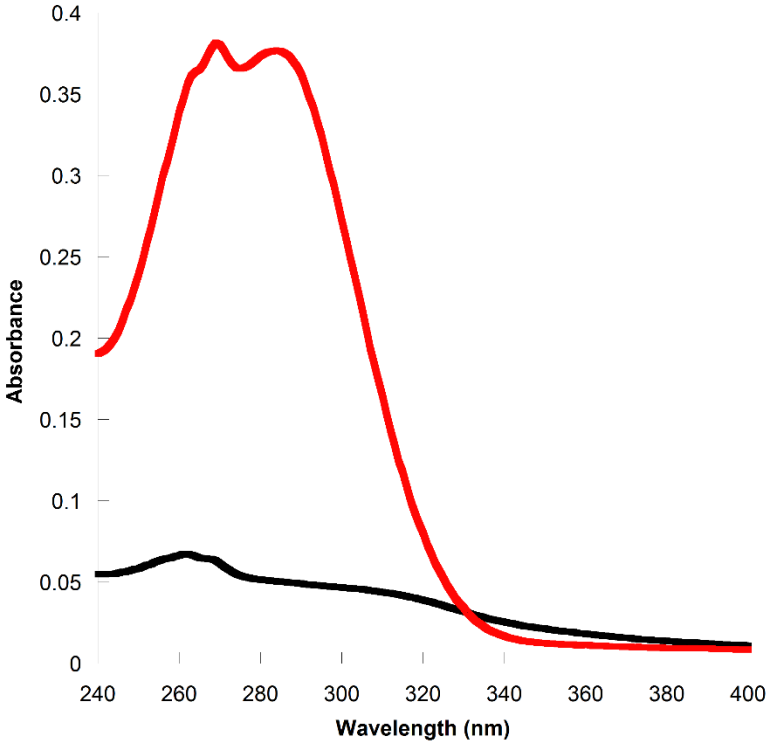

Figure B.1. UV-Vis spectra of original solution of L-PO_3H_2 (red) and supernatant collected after stirring with $SrTiO_3$ (black). Difference in absorbance at 295 nm used to determine moles of ligand immobilized on $SrTiO_3$.

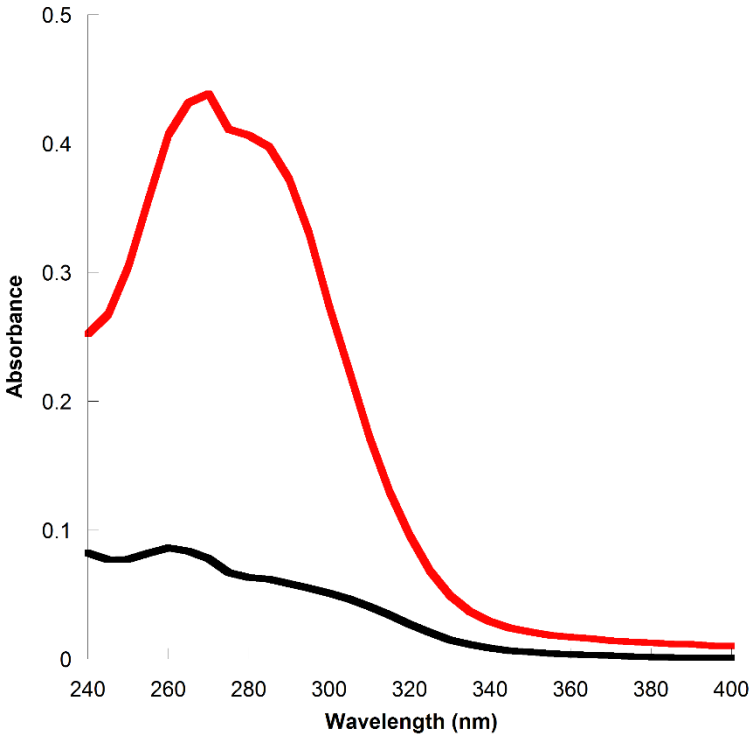

Figure B.2. UV-Vis spectra of original solution of L-PO_3H_2 (red) and supernatant collected after stirring with TiO_2 (black). Difference in absorbance at 295 nm used to determine moles of ligand immobilized on TiO_2.

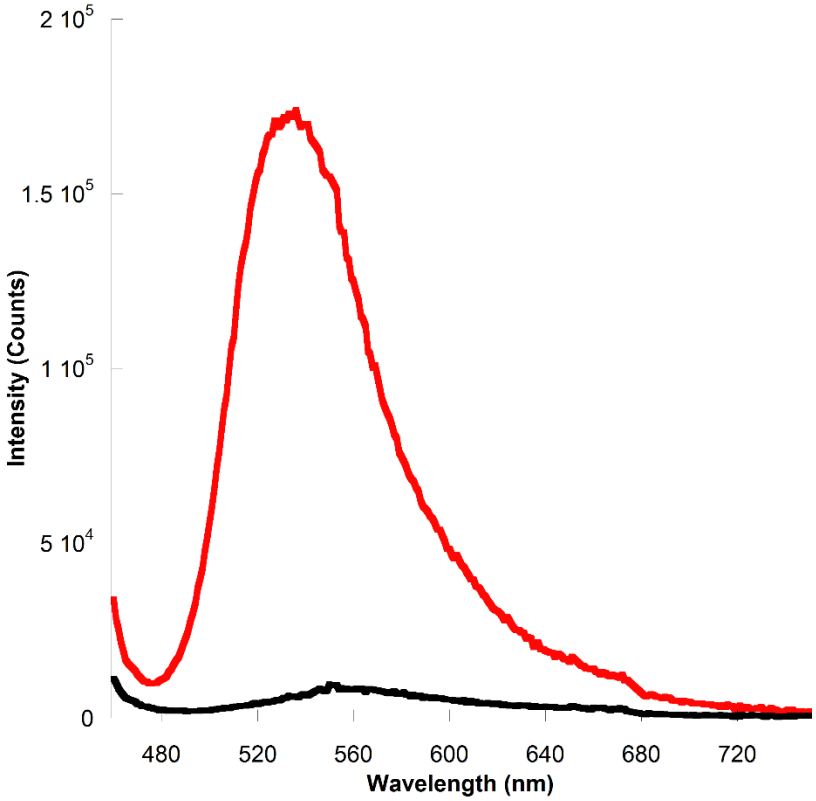

Figure B3. Emission spectra of fluorescein on $SrTiO_3$ (red) and fluorescein on TiO_2 (black).